



Steam pretreatment of bone char for adsorption of refractory organics from electro dialysis concentrate produced by petroleum refinery

Felipe de Aquino Lima¹ · Isabel Pereira da Silva¹ · Paula Valamiel de Oliveira Vieira¹ · Sônia Denise Ferreira Rocha² · Patrícia da Luz Mesquita¹

Received: 24 December 2022 / Accepted: 17 November 2023 / Published online: 9 December 2023
© The Author(s), under exclusive licence to Springer-Verlag GmbH Germany, part of Springer Nature 2023

Abstract

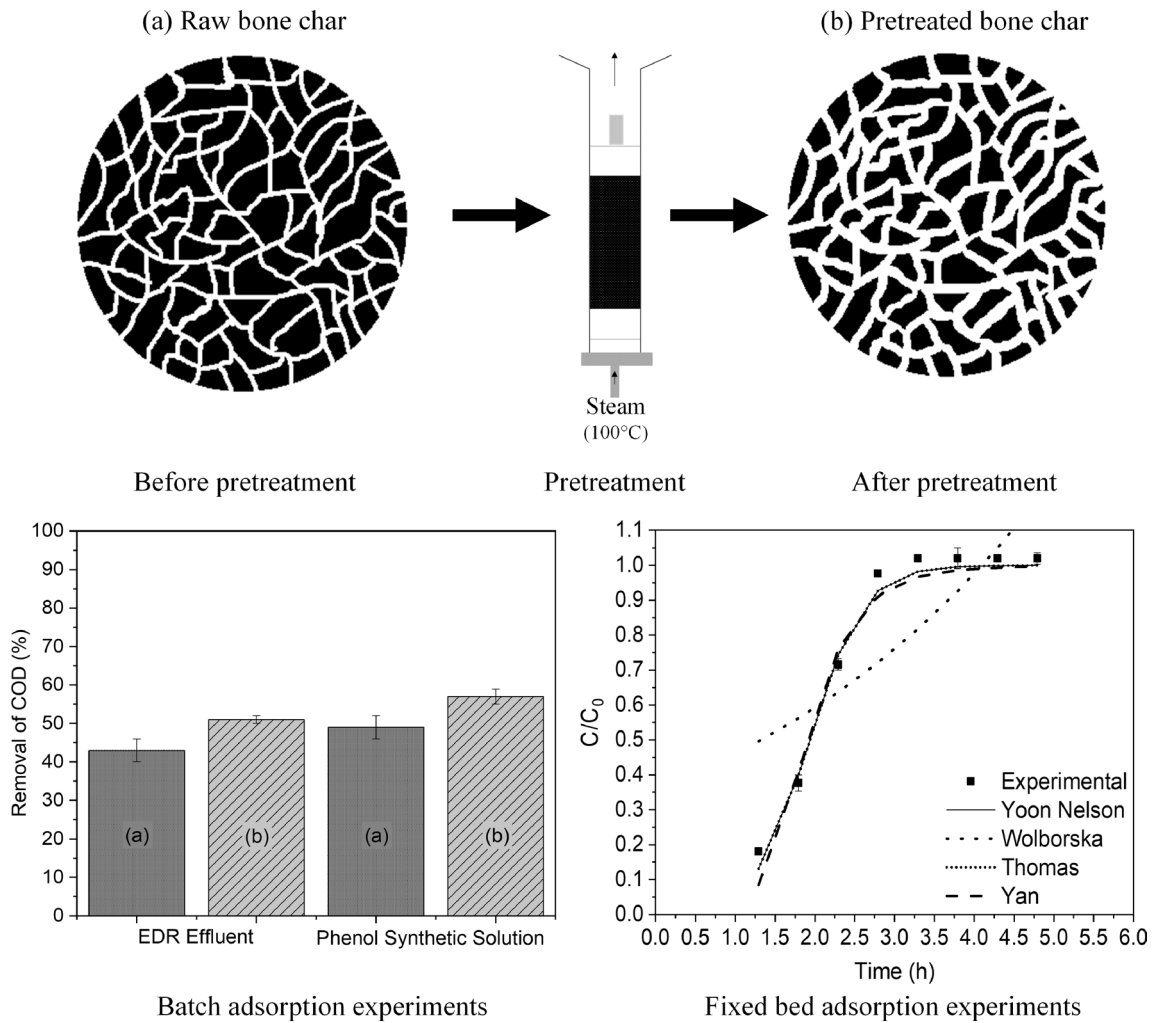
Water reuse has been gaining strength with a focus on sustainability issues and the water crisis. However, as water recirculates in the processes, the demand for the removal of refractory compounds comes up, some toxics even at small concentrations. To maximize the possibilities of water reuse, a steam pretreatment at 98 ± 2 °C for bone char used as adsorbent is proposed to improve refractory organic compounds removal from refinery wastewater. In this study, raw and steam-pretreated bone char (0.5–1.4 mm) were used to remove refractory organics from a petroleum refinery reverse electro dialysis (EDR) effluent (COD: 60 mg L⁻¹) and phenol from a synthetic solution (COD: 47 mg L⁻¹). In addition to solid characterization analysis, bench-scale tests in batch and semi-continuous systems were carried out, using an orbital shaker and fixed-bed column, respectively. The pretreatment provided a greater surface area, porosity, and adsorptive capacity to the bone char, in comparison to the raw one. In batch tests, the adsorptive capacity of the pretreated bone char was 15 and 19% higher than raw bone char, applying EDR effluent and phenol synthetic solution, respectively. The semi-continuous test for phenol removal using pretreated bone char provided a breakthrough curve with the expected sigmoidal format and was best described by the models of Yoon and Nelson ($R^2=0.9836$), Yan ($R^2=0.96705$), and Thomas ($R^2=0.9836$). The adsorptive capacity values of 2.99 mg g⁻¹ and 2.88 mg g⁻¹ from batch and semi-continuous tests, respectively, were close for phenol removal using pretreated bone char.

✉ Felipe de Aquino Lima
felipeaquinolima@gmail.com

¹ Department of Chemical Engineering, Federal University of São João del-Rei, Campus Alto Paraopeba, Fazenda do Cadete, Ouro Branco, MG, Brazil

² Department of Mining Engineering, Universidade Federal de Minas Gerais, Pampulha, Belo Horizonte, Brazil

Graphical abstract



Keywords Bone char · Steam pretreatment · Adsorption · Refractory organics · Phenol · Water reuse

Introduction

Population growth coupled with industrial development increases the demand for clean and quality water while contributing to the increased wastewater generation. To reduce the effects of water pollution from anthropogenic causes, the effluent treatment plants utilization, especially for organic load and toxicity removal, is essential (Adamiak 2013; Turek et al. 2017; Mesquita et al. 2017; Rashid et al. 2021). In addition, objectives 6 and 12 of the United Nations 2030 Agenda for Sustainable Development encourage the sustainable management of water and natural resources consumption patterns, wastewater treatment, and water reuse as the best way of consuming this resource (United Nations 2015). Reuse practices avoid new catchments and allow a cleaner and economically advantageous production process.

However, the recirculation of effluents in the process can result in some contaminants enrichment in water.

In this context, it is important to explore effluent reuse alternatives in petroleum refineries, one of the most relevant industrial sectors. This industrial process uses an average of 246–340 L of water per barrel of crude oil processed and, consequently, generates effluent volumes around 0.4–1.6 times the processed oil volume (Alva-Argáez et al. 2007). The treatment of this volume of effluent generally involves the removal of contaminants such as oil and suspended solids by physical–chemical processes, followed by biological processes for organics and nitrogen removal (Domingos and Fonseca 2018).

The third stage of effluent treatment, usually called tertiary treatment, is essential in petroleum refineries to make the effluent appropriate for disposal or reuse in the

process. Currently, one of the most used technologies is reverse electro dialysis (EDR), allowing wastewater desalination for reuse in the process, but presenting the generation of saline concentrate flows as a disadvantage (Choi and Kim 2015; Chong et al. 2015; Tang et al. 2016; Wang et al. 2023). Focused on that, the crystallization would be an applicable technology for the management of EDR's saline concentrate flow, separating the salts in the solid state and allowing their final disposal in landfills, for example. However, refractory contaminants, such as organics compounds, present in EDR's effluent may influence the crystallization process, decreasing its performance and the quality of the final products (Randall et al. 2011; Becheleni et al. 2017).

In addition to harming processes such as crystallization, the refractory compounds dissolved in the EDR effluent have a high polluting potential and generate great concerns about their toxicity and carcinogenicity (Becheleni et al. 2015). Several organic contaminants have already been found on the EDR saline concentrate, such as long-chain hydrocarbons, benzenic and phenolic aromatic compounds, amines, and amides (Becheleni et al. 2015; Mesquita et al. 2017; Mesquita et al. 2018b). In their study about the application of a fixed bed of bone char for refractory organics removal from the EDR concentrate by adsorption, (Mesquita et al. 2018b) identified about 70 different refractory organic compounds on this effluent.

Phenol has been declared a hazardous contaminant and placed on the priority pollutant list by the United States Environmental Protection Agency (EPA) due to its acute toxicity to living organisms, carcinogenicity, corrosivity, and potential damage to ecological systems even at low concentrations (Li et al. 2018; Panigrahy et al. 2022). The traditional techniques of phenol removal mainly include membrane separation processes, reverse osmosis, chemical and electrochemical oxidative processes, coagulation, photooxidation, biodegradation, and solvent extraction (Vourch et al. 2008; Cristóvão et al. 2015; Abbassian et al. 2015; Mesquita et al. 2018b; Silva et al. 2018).

Adsorption is also an effluent treatment alternative, being one of the most widely studied technologies (Maria and Mansur 2017; Kennedy and Arias-Paic 2020; Villela-Martínez et al. 2020; Maeng et al. 2020; Coltre et al. 2020; Pérez Jiménez et al. 2021; Liu et al. 2021; Sellaoui et al. 2021; Li et al. 2022; Moussavi et al. 2022; Yang et al. 2022; Valverde et al. 2022). Its operational simplicity and high selectivity, requiring low energy consumption are important features to highlight. The use of commercial activated carbon as an adsorbent is common in some industrial sectors, however, its high cost often makes its large-scale application unfeasible. Research on lower-cost adsorbents as an alternative to activated carbon has become increasingly frequent. The bovine bone, a bulky waste of meat processing

companies, has been reported as a potential raw material for the synthesis of an alternative activated carbon, the bone char (Cazetta et al. 2014; Patel et al. 2015; Geça et al. 2022; Hart et al. 2023).

Bone char is a solid granular material produced by the calcination of animal bones, where they are heated to a temperature up to 800 °C with a controlled oxygen supply (Rocha et al. 2012; Nigri et al. 2017b). The main bone char inorganic component is the calcium phosphate, in hydroxyapatite (HAP) form. Therefore, bone char is distinguished from other common adsorbents by its composition of 80–90% calcium phosphate and only about 10%w carbon (Patel et al. 2015; Azeem et al. 2022; Medellín Castillo et al. 2023). Many studies assess bone char as an adsorbent for synthetic solutions treatment, as for fluoride (Brunson and Sabatini 2014; Nigri et al. 2017b), crystal violet (Cruz et al. 2020), methylene blue (Ghanizadeh and Asgari 2011), sodium dodecyl sulfate (Hashemi et al. 2013), boron (Valverde et al. 2022), and ions removal (Moreno et al. 2010), but they are rare for organic compounds and real wastewater.

A study developed by Mesquita et al. (2018a) about steam regeneration of bone char for removal of refractory organics, in terms of chemical oxygen demand (COD), showed promising results. Bone char was saturated with EDR saline concentrate wastewater, being the refractory organics quantified as COD, and, then, regenerated by steam in a bench-scale fixed-bed column. The tests were performed alongside a 10-cm bed of saturated bone char in contact with steam for 30 min, with the steam flow and temperature of 0.6 g.min⁻¹ and 96 ± 0.5 °C, respectively. Under these conditions, a recovery greater than 132% was identified. The regeneration provided a greater COD removal by the regenerated bone char than the raw adsorbent at the saturation test. This indicated that, besides the regeneration, the steam pretreated the bone char. Therefore, it would be interesting to investigate if the possible steam pretreatment improved the bone char properties related to its adsorption capacity.

Some studies analyze steam pretreatment of adsorbents and char in general, most of which are using high pressures or high temperatures. Li et al (2017) evaluated this technique (700 °C, 2 h) to improve the surface properties of activated carbon for high-performance supercapacitors. They observed by the adsorption–desorption isotherms of N₂ that the pretreatment produced highly mesoporous coal, differently from the raw one. In addition, their steam pretreatment significantly increased the surface area and pore volume of the activated carbon. He et al. (2020) investigated the saturated steam treatment (180–200 °C, 5–10 min) of rice straw pellets in moisture sorption tests. They found that there was an increase in carbon content, a decrease in oxygen, and a decrease in the contents of cellulose, hemicelluloses, and lignin. The

pretreatment process allowed the improvement of the caloric values and increased the hydrophobicity of rice straws.

Several authors used autoclaves to produce steam, as in the work of Xu et al. (2020) evaluated a pretreatment with high-pressure vapor (autoclave at 130 °C, 40 min) followed by a step heating (350 °C, 3 h, different heating rates) in electrospun fibers of SiO₂–MgO used in an adsorption study of Pb(II) and Cu(II). The authors suggested that high-pressure vapor promoted an involution of the structure and gave the fiber a homogeneous body and pore-rich surface. Parvin et al. (2017) used the steam pretreatment (autoclave a 121 °C, 40 min) in jute stick powder for blue dye removal from textile effluent, obtaining an efficiency almost 30% greater than the raw adsorbent. According to them, the pretreatment allowed the surface area to increase and exposed more functional groups related to the adsorptive capacity. Robinson et al. (2002) performed a steam pretreatment (autoclave at 121 °C, 15 min) in wheat straw, corncobs, and barley husks for dye adsorption and also observed an increased surface area of the straw by high-pressure heating and had a high final percentage of dye removed. Yang and Cannon (2022) used steam bursting pretreatment (160 °C, 300–700 psi, 5 min) of biomass-activated carbon derived from pine sawdust for the adsorption of perfluorooctanoic acid and methylene blue. The authors performed subsequent pyrolysis of this material. The characterization showed that the specific surface areas and micropore volumes decreased with the increase in pressure. Nascimento and Barros Neto (2021) also used high pressures in a hydrothermal pretreatment steam explosion process (210 °C, 5 bar, 15 min) in coconut husk adsorbents for the removal of Cu²⁺ and Cd²⁺. It has been verified that thermal degradation of hemicellulose has occurred, with an increase in biomass crystallinity and porosity, favoring the adsorption.

The use of high pressures and temperatures makes the process more expensive and difficult. The use of steam in batch processes was used in all the works mentioned above. An industry application would require the flow of steam in a continuous process, such as in a fixed bed, employing a column. To the best of our knowledge, no previous study has been dedicated to assessing steam pretreatment around 100 °C on improving bone char capacity to remove refractory COD from phenol synthetic solution and petroleum refinery EDR effluent, and this is the main contribution of this work.

Materials and methods

Bone char preparation and selection

The bone char was provided by Bonechar Carvão Ativado do Brasil Ltda, located in Maringá—PR. The material was

produced by calcination at 700 °C for 8 h (BONECHAR 2018). The total sample was quartered to obtain representative aliquots according to Brazilian technical standards of field sample reduction for laboratory tests (ABNT 2001).

The particle size analysis was performed using a vibrating system (Bertel Indústria Metalúrgica Ltda) with sieves of 6, 12, 32, 48, 60, and 100 mesh for 15 min at 5 rpm. Bone char (12–32 mesh or 0.5–1.4 mm) was selected for the adsorption tests. The material was washed four times with distilled water in a ratio of 250:1 (grams of bone char:liters of water) for adhered fines removal. Finally, the bone char was dried in a furnace (Sterilifer SX1.1 DTME, serial number 0057) at 120 °C for 2 h to dry (Mesquita et al. 2018a).

Steam pretreatment

Bone char steam pretreatment is carried out in the experimental setup as shown in Fig. 1. The steam generation system had a vertical glass column (20 cm high, diameter of 0.7 cm) inside which a 10-cm bone char bed (average mass of 1.89 ± 0.50 g) was packaged between two layers of cotton. A rubber tube was used to connect the glass tube bottom to a flask containing 400 mL of water. The flask was kept under stirring and heating (Magnetic Stirrer Fisatom, 752A) generating steam at 98 ± 2 °C. In the flask's upper hole, a rubber stopper was used to attach a thermometer. The steam was applied to the bone char bed in a ratio of 13:1 (grams of steam:grams of bone char) and at an average flow of 0.8 ± 0.2 g min⁻¹. Finally, the pretreated bone char was washed four times with distilled water in a ratio of 250:1 (grams of bone char:liters of water) and dried on a moisture meter with an infrared heat source (Marte V1.8, ID50).

Bone char characterization

The bulk density (ρ_A) of the bone char fraction selected for the tests was determined according to Brazilian technical standards of determination of apparent specific mass (ABNT 1991). Both raw and pretreated bone char surface area and porosity were determined by N₂ adsorption–desorption analysis (Nova 1200e) at a preparation temperature of 80 °C under a vacuum. From the obtained isotherm, the specific surface area and average pore diameter were determined using the BET method, the volume of micropores by the t-plot method, and total pore volume as defined by the corresponding amount of adsorbed N₂ with relative pressure $p/p_0 = 0.99$. The morphology of bone char before and after pretreatment was evaluated using a scanning electron microscope (FEI Magellan 400 L). The samples were fixed in the sample holders with carbon tape, followed by a coating with gold for 90 s (Balzers Sputter Coater SCD 004 and Union CED

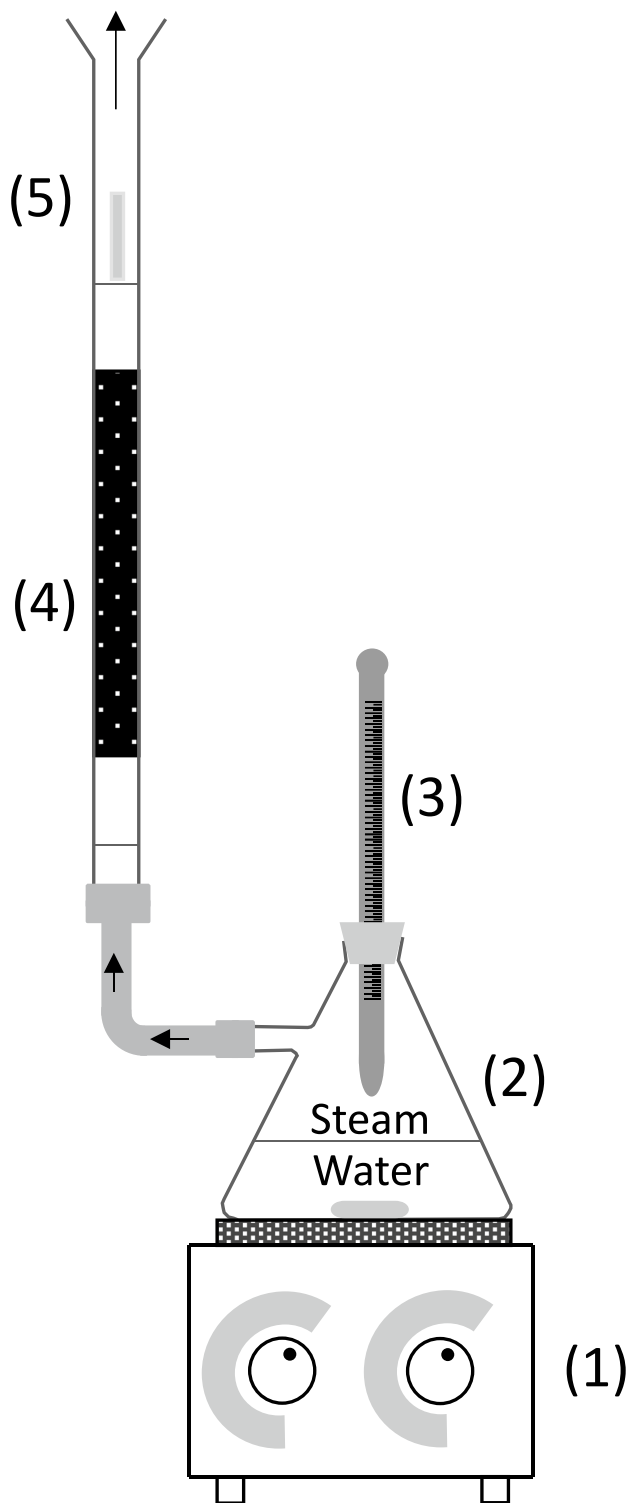


Fig. 1 Steam generation system for bone char pretreatment in bench scale: (1) magnetic stirrer with heating; (2) water under heating and stirring; (3) thermometer; (4) bone char fixed bed; (5) glass column

020). Bone char ash content was performed according to Brazilian technical standards for the determination of ash content in mineral coal (ABNT 2017). Crystalline phases were determined by X-ray diffraction (XRD) in a Rigaku diffractometer (Miniflex 600) operating with Cu K α radiation. The goniometer velocity was $0.5^\circ \text{ min}^{-1}$ to the crystalline phases detection in angles from 5° to 80° . To determine the point of zero charge (PZC), the 11-point experiment described by (Robles and Regalbuto 2004) was used. The bone char pH was measured using the methodology described by (Huff and Lee 2016), adding 1 g of char to 10 ml of distilled water, under agitation at 110 rpm and 28° C for 1 h and subsequently measuring the pH of this solution using a Digimed DM-22 pHmeter. Both methodologies, for PZC and pH, were applied using a refrigerated shaker incubator (New Technique, NT715) and a pH meter (Digimed DM-22). The thermogravimetric analysis (TGA) for evaluation of mass loss was performed in a DTG-60H analyzer (serial number C30574800329TK) with N $_2$ gas (flow of 50 mL min^{-1}) and heating rate of $10^\circ \text{ C min}^{-1}$, from 30 to 900° C . Fourier transformed infrared spectroscopy (FTIR) (Bruker FTIR Alpha, serial number 100413) was used to identify the surface groups on the bone char samples prepared on KBr anidre disk.

EDR effluent characterization

The effluent was sampled in the field, from the petroleum industry reverse electro dialysis (EDR) feeding stream, conditioned into 20 L flasks, and sent to the laboratory, where it was fractionated into 1 L flasks and temporarily stored at 4° C in a refrigerator.

For EDR effluent characterization, parameters such as conductivity, bicarbonate alkalinity, total alkalinity, aluminum, barium, calcium, chloride, chemical oxygen demand (COD), strontium, total phosphorus, magnesium, nitrogen, potassium, sodium, sulfate, and total suspended solids were determined according to the Standard Methods for the Examination of Water and Wastewater (APHA 2017). The pH and turbidity were determined using a pH meter (Digimed DM-22) and turbidimeter (Hanid HI 98703), respectively. The refractory organics concentration in the EDR effluent was measured in terms of chemical oxygen demand (COD), according to the closed reflux colorimetric method for low-concentration range (APHA 2017), using dry block (Policontrol, serial number 331) and spectrophotometer (AJX-1600, serial number VED 1111006). Potassium bi-phthalate standard at concentrations of 0, 10, 20, 30, 40, and 60 mg L^{-1} was used for the analytical curve.

Phenol synthetic solution preparation

A 47 mg L⁻¹ phenol synthetic solution was used to simulate the EDR effluent for laboratory preliminary adsorption tests. This concentration was based on the fact that the petroleum refinery EDR effluent had a COD of approximately 60 mgO₂ L⁻¹. Phenol (C₆H₅OH—Sigma-Aldrich) was previously melted in a 60 °C water bath. As performed for the EDR effluent, the phenol synthetic solution concentration was measured in terms of COD (APHA 2017).

Bench-scale adsorption experiments

Batch system

The batch experiments on bench scale were carried out in triplicates under the same conditions for 4 systems: (1) raw bone char—phenol synthetic solution; (2) pretreated bone char—phenol synthetic solution; (3) raw bone char—EDR effluent; (4) pretreated bone char—EDR effluent. The tests were conducted under stirring and controlled temperature (Nova Técnica refrigerated shaker incubator, NT715), 200 ± 1 rpm and 25 °C, respectively, for 4 h. A solid–liquid ratio of 10:1 (grams of bone char:liter of fluid phase) was used in all the tests and the final organic concentration, in terms of COD, was determined for the EDR effluent (APHA 2017). The pH of the fluid phases was monitored (pH meter Digimed DM-22) and was 7.1 ± 0.2 for the phenol synthetic solution and 7.3 ± 0.1 for the EDR effluent.

Semi-continuous system

A preliminary test for phenol removal by pretreated bone char in a semi-continuous system, using a fixed-bed column on a bench scale, was carried out in the setup illustrated in Fig. 2. The phenol synthetic solution was kept under stirring by a magnetic stirrer (Thelga, serial number 02019-0413-003120) and pumped (peristaltic pump Instruments SA—Spetec Pennex 12/2, serial number 03006773) upward through the fixed bed of pretreated bone char. Pretreated bone char mass (*m*) was packaged between two layers of glass spheres in a 7 mm diameter (Ø) glass column. Phenol synthetic solution at the column outlet was automatically sampled every 30 min and phenol concentration, in terms of COD, was determined for the EDR effluent.

The experimental conditions in which the preliminary test for phenol removal by pretreated bone char in a semi-continuous system, using a fixed-bed column on a bench scale, was carried out are presented in Table 1. The phenol synthetic solution temperature and pH (pH meter Digimed

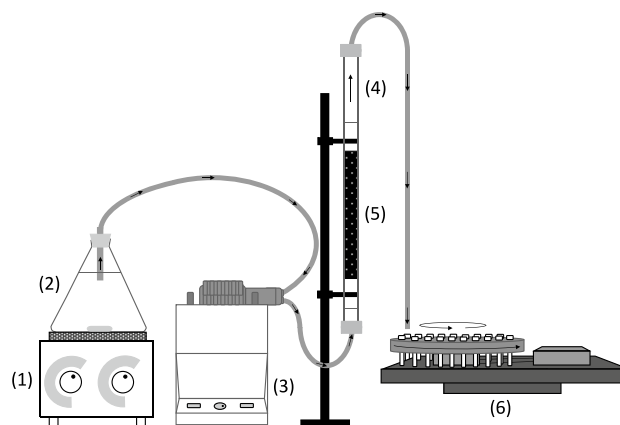


Fig. 2 Semi-continuous system for phenol removal by adsorption onto pretreated bone char in bench-scale fixed-bed column: (1) magnetic stirrer; (2) phenol synthetic solution under stirring; (3) peristaltic pump; (4) glass column; (5) pretreated bone char fixed-bed column; (6) automated sampling system

Table 1 Experimental conditions for phenol removal test by adsorption onto pretreated bone char in bench-scale fixed-bed column

Operational conditions		Values
Column length-to-diameter ratio	$h/\text{Ø}$	7.8
Bed depth	h [cm]	5.5
Bed mass	m [g]	1.2031
Superficial velocity	Q_s [m ³ m ⁻² h ⁻¹]	0.80
Volumetric flow rate	Q [mL min ⁻¹]	0.51 ± 0.02
Initial concentration	C_0 [mgO ₂ L ⁻¹]	58.9 ± 1.5

DM-22) were monitored (7.2 ± 0.1 and 23.5 ± 0.5 °C, respectively).

A breakthrough curve was obtained for this semi-continuous experiment as the relative concentration (C/C_0) versus the time (t), where C is the concentration at time t , and C_0 is the initial concentration. The breakthrough point was determined considering 5% more than the minimum C/C_0 and the exhaustion point considering 95% of the maximum C/C_0 (Worch 2012; Metcalf et al. 2014; Xavier 2018; Mesquita et al. 2018b).

The adsorptive capacity (q_0) was determined by applying a mass balance equation (Eq. 1) to the breakthrough curve and assuming: (1) no formation or consumption reactions; (2) the experimental conditions of bed mass (m) and initial concentration (C_0); (3) the adsorbate either adhered onto the adsorbent or remained in the fluid phase; (4) the empty bed volume (V_L) filled by the fluid phase, determined by the difference between the bed total volume and the bed volume filled by the adsorbent mass, considering its apparent density (ρ_A); (5) the area above the breakthrough curve, in terms of time (t), related

to the adsorptive capacity (q_0) (Worch 2012; Metcalf et al. 2014; Xavier 2018).

$$q_0 \cdot m + C_0 \cdot V_L = C_0 \cdot Q \cdot \int_{t=0}^{t=\infty} \left(1 - \frac{C}{C_0}\right) dt \quad (1)$$

where q_0 is the adsorptive capacity, m is the bed mass, C_0 is the initial concentration, V_L is the bed volume filled by the liquid phase, Q is the volumetric flow rate, t is the time, and C/C_0 is the relative concentration.

The adsorptive capacities up to the breakthrough (q_B) and exhaustion (q_E) points could be determined using Eq. (1) and assuming the time interval from zero up to the breakthrough (t_B) or exhaustion (t_E) time, respectively.

The operational and dynamic parameters that describe the breakthrough curve behavior and the adsorption process were calculated using the operational conditions (Table 1), the information contained in the obtained breakthrough curve, and Eqs. (2)–(19) presented in Table 2 (Reynolds and Richards 1995; Worch 2012; Metcalf et al. 2014; Nascimento et al. 2014; Harrison et al. 2015; Xavier 2018; Mesquita et al. 2018b).

where \emptyset is the column diameter, h is the bed depth, m is the bed mass, ρ_A is the adsorbent apparent density, m_A is the adsorbent particle mass, Q is the volumetric flow rate, q_B is

the adsorptive capacity up to the breakthrough time (t_B), q_E is the adsorptive capacity up to the exhaustion time (t_E), V_B is the column breakthrough volume, and V_E is the column exhaustion volume.

The modeling of the breakthrough curve obtained in the semi-continuous test for phenol adsorption onto pretreated bone char was performed by Thomas, Yoon and Nelson, Yan, and Wolborska models fit the experimental data using the Eqs. (20)–(25) presented in Table 3 (Thomas 1944; Yoon and Nelson 1984; Yan et al. 2001; Xu et al. 2013;

Table 3 Models fitted to the breakthrough curve of phenol adsorption onto pretreated bone char

Models	Equations
Thomas	$\frac{C}{C_0} = \frac{1}{1 + \exp\left[\frac{k_T}{Q}(q_T \cdot m - C_0 \cdot Q \cdot t)\right]}$ (20)
Yoon and Nelson	$\frac{C}{C_0} = \frac{1}{1 + \exp[K_{YN} \cdot (\tau \cdot t)]}$ (21)
Yan	$\frac{C}{C_0} = 1 - \frac{1}{1 + \left(\frac{Q}{b}\right)^{aY}}$ (22)
	$b = \frac{q_Y \cdot m}{C_0}$ (23)
Wolborska	$\frac{C}{C_0} = \exp\left[\left(\frac{\beta_a \cdot C_0}{N_0}\right)t - \frac{\beta_a \cdot h}{Q_S}\right]$ (24)
	$\beta_a = \frac{Q_S^2}{2D} \left(\sqrt{1 + \frac{4\beta_0 \cdot D}{Q_S^2}} - 1\right)$ (25)

Table 2 Equations used to calculate the adsorption breakthrough curve operational and dynamic parameters

Parameters		Equations	
Operational	Bed volume	V_R [mL]	$V_R = \pi \cdot \left(\frac{\emptyset}{2}\right)^2 \cdot h$ (2)
	Bed volume filled by the adsorbent mass	V_A [mL]	$V_A = \frac{m}{\rho_A}$ (3)
	Empty bed volume	V_L [mL]	$V_L = V_R - V_A$ (4)
	Bed density	ρ_R [g cm ⁻³]	$\rho_R = \frac{m}{V_R}$ (5)
	Bed porosity	ϵ_R [%]	$\epsilon_R = 1 - \frac{\rho_B}{\rho_A}$ (6)
	Bed adsorbent particle number	Z_A	$Z_A = \frac{m}{m_A}$ (7)
	Fluid phase superficial velocity	Q_S [cm min ⁻¹]	$Q_S = \frac{Q}{\pi \cdot \left(\frac{\emptyset}{2}\right)^2}$ (8)
	Effective fluid phase velocity	Q_E [cm min ⁻¹]	$Q_E = \frac{Q_S}{\epsilon_R}$ (9)
	Empty bed contact time	EBTC [min]	$EBCT = \frac{h}{Q_S}$ (10)
	Effective fluid phase residence time	t_R [min]	$t_R = EBCT \cdot \epsilon_R$ (11)
Dynamic	Process efficiency	η [%]	$\eta = \frac{q_B}{q_0}$ (12)
	Effective bed use	h_E [cm]	$h_E = \frac{q_B}{q_E} \cdot h$ (13)
	Length of unused bed	LUB [cm]	$LUB = \left(1 - \frac{q_B}{q_E}\right) \cdot h$ (14)
	Mass transfer zone movement time	t_M [min]	$t_M = t_E - t_B$ (15)
	Fractional adsorbent capacity	F	$F = \frac{\int_{V_B}^{V_E} (C_0 - C) dV}{C_0 \cdot (V_E - V_B)}$ (16)
	Mass transfer zone formation time	t_F [min]	$t_F = (1 - F) \cdot t_M$ (17)
	Mass transfer zone height	h_Z [cm]	$h_Z = \frac{t_M}{t_E - (1 - F) \cdot t_M} \cdot h$ (18)
	Mass transfer zone movement rate	U_Z [cm h ⁻¹]	$U_Z = \frac{h_Z}{t_M}$ (19)

Nascimento et al. 2014; Mesquita et al. 2018b; Santos et al. 2020; Cruz et al. 2020).

where C is the concentration at time t , C_0 is the initial concentration, K_T is the Thomas rate constant, Q is the volumetric flow rate, q_T is the adsorptive capacity from the Thomas model, m is the bed mass, K_{YN} is the Yoon and Nelson constant, τ is the time required for the adsorbent to reach the relative concentration (C/C_0) equal to 0.5, a_Y is the Yan constant model, q_Y is the adsorptive capacity from Yan model, β_α is the external mass transfer kinetic coefficient, N_0 is the mass transfer capacity, h is the bed depth, Q_S is the fluid phase superficial velocity, D is the axial diffusion coefficient, and β_0 is the external mass transfer kinetic coefficient for negligible axial diffusion coefficient.

The mathematical models fit the experimental data were evaluated using the determination coefficient (R^2) (Eq. 26), the average absolute deviation (%D) (Eq. 27), and the corrected Akaike information criteria (AIC_C) (Eq. 28) (Bonate 2011; Santos et al. 2020).

$$R^2 = 1 - \frac{\sum_{i=1}^N (q_{\text{exp}} - q_{\text{pred}})^2}{\sum_{i=1}^N (q_{\text{exp}} - \bar{q})^2} \quad (26)$$

$$\%D = \left(\frac{1}{N} \sum_{i=1}^N \left| \frac{q_{\text{exp}} - q_{\text{pred}}}{N} \right| \right) \cdot 100\% \quad (27)$$

$$AIC_C = N \cdot \ln \left(\sum_{i=1}^N \frac{(q_{\text{exp}} - q_{\text{pred}})^2}{N} \right) + 2p + \frac{2p(p+1)}{N-p-1} \quad (28)$$

where N is the number of experimental data, q_{exp} is the amount of adsorbate removed experimentally (mg g^{-1}); q_{pred} is the amount of adsorbate removed predicted (mg g^{-1}); \bar{q} is the average of the observed values (mg.g^{-1}) and p is the number of parameters in the model + 1.

Results and discussion

Bone char characterization

The bone char apparent density (ρ_A), measured from the sample selected for the tests, was 0.68 g cm^{-3} , within the range reported by the supplier (0.6 to 0.7 g cm^{-3}) (BONECHAR 2018). Based on the granulometry of the bone char sample selected for the tests, between 0.5 and 1.4 mm , it was assumed that the adsorbent particles have an average diameter (ϕ_A) of 0.95 mm . Considering the adsorbent particles as spherical, the values of average radius

(r_A) of 0.475 mm , surface area (A_A) of 2.84 mm^2 , and unit mass (m_A) of 0.31 mg were calculated.

The characteristics of surface area, total porous volume, and average porous diameter determined by N_2 adsorption–desorption tests for both raw and pretreated bone char are shown in Table 4. The physisorption of N_2 for the bone char sample is shown in Fig. 3. The obtained adsorption/desorption isotherm is classified as a type-V isotherm, according to the IUPAC technical report about the classification of physisorption isotherms, whereas the hysteresis is of the type H3, indicating the predominance of mesopores in the form of parallel plates (Thommes et al. 2015). In this type of isotherm, in low P/P_0 ranges, relatively weak interactions of micro or mesoporous adsorbents with adsorbate are present, and as partial pressures increase, molecular clustering is followed by pore filling (Thommes et al. 2015; Mesquita et al. 2017).

Both bone char samples presented a surface area in the literature reported range. For raw bone char, surface areas of $90 \text{ m}^2 \text{ g}^{-1}$ (Mesquita et al. 2017), $119 \text{ m}^2 \text{ g}^{-1}$ (Ribeiro 2011), and $139 \text{ m}^2 \text{ g}^{-1}$ (Nigri et al. 2017a) were found in research that used bone char from the same supplier. Despite the short porous length found, a typical mesoporosity is present for both bone char samples, according to the IUPAC classification (2 to 50 nm). Works in the literature (Tovar-Gómez et al. 2013; Rojas-Mayorga et al. 2015; Nigri et al. 2017b; Mesquita et al. 2017) reported this mesoporous characteristic for the raw bone char.

Bone char steam pretreatment affected its surface area, total pore volume, and average pore diameter providing increases of 4% , 11% , and 9% , respectively, in comparison to the raw bone char. Similar studies using steam pretreatment for bone char were not found in the literature for direct comparison of the results obtained. Figure 4 shows a schematic representation of the effect of pretreatment in those parameters and SEM images before and after the pretreatment. The images corroborate the previous findings, with a visible increase in the number and diameter of the pores with the pretreatment. Lebigue et al. (2010) used a steam flow of 0.7 g min^{-1} at temperatures between 200 and $1000 \text{ }^\circ\text{C}$ on sewage sludge samples carbonization and obtained a surface area increase between 24 and 47% and a porous diameter increase between 2 and 29% . Gangupomu et al. (2016)

Table 4 Surface area, total porous volume, and average porous diameter determined by the N_2 adsorption–desorption tests for raw and pretreated bone chars

Parameters		Raw bone char	Pretreated bone char
Surface area	$[\text{m}^2 \text{ g}^{-1}]$	95.8	99.7
Total porous volume	$[\text{cm}^3 \text{ g}^{-1}]$	0.27	0.30
Average porous diameter	$[\text{nm}]$	2.8	3.1

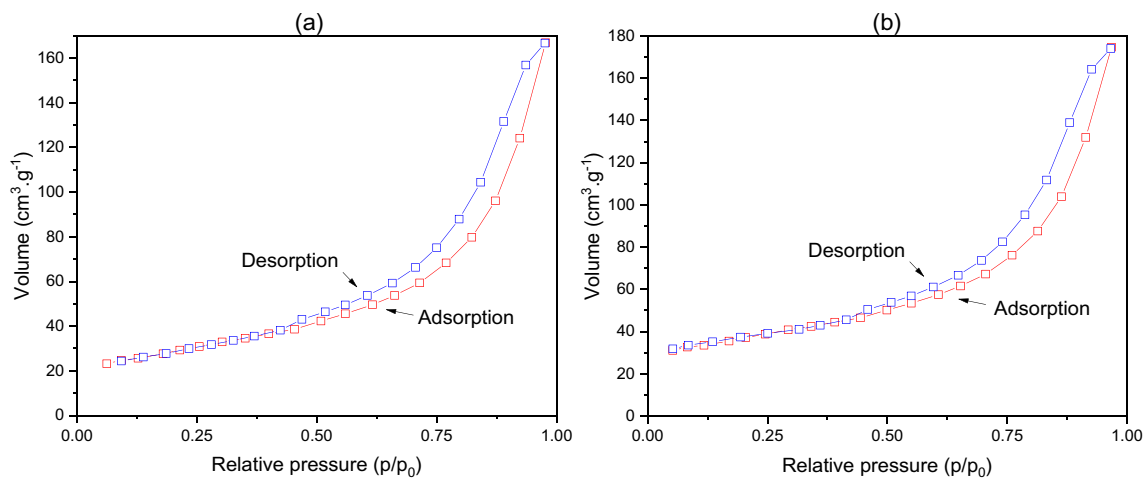


Fig. 3 Nitrogen isotherms of **a** raw and **b** pretreated bone chars

applied steam pretreatment at 400 °C followed by nitric acid treatment for 3–12 h onto carbon nanotubes and obtained a surface area increase in approximately 18%, a 42% increase in the average pore diameter and a total pore volume of 8%.

Aiming at a better comprehension of the bone char properties affected by the steam pretreatment, characteristics such as ash content, crystalline structures, point of zero charge (PZC), pH, and loss of mass with temperature and surface groups were also analyzed. The ash content found for raw and pretreated bone char was 80.8 ± 0.2 and $80.5 \pm 0.6\%$, respectively. This result corroborates the majority composition of bone char by inorganic compounds, especially calcium phosphate in the form of hydroxyapatite (Mesquita et al. 2017).

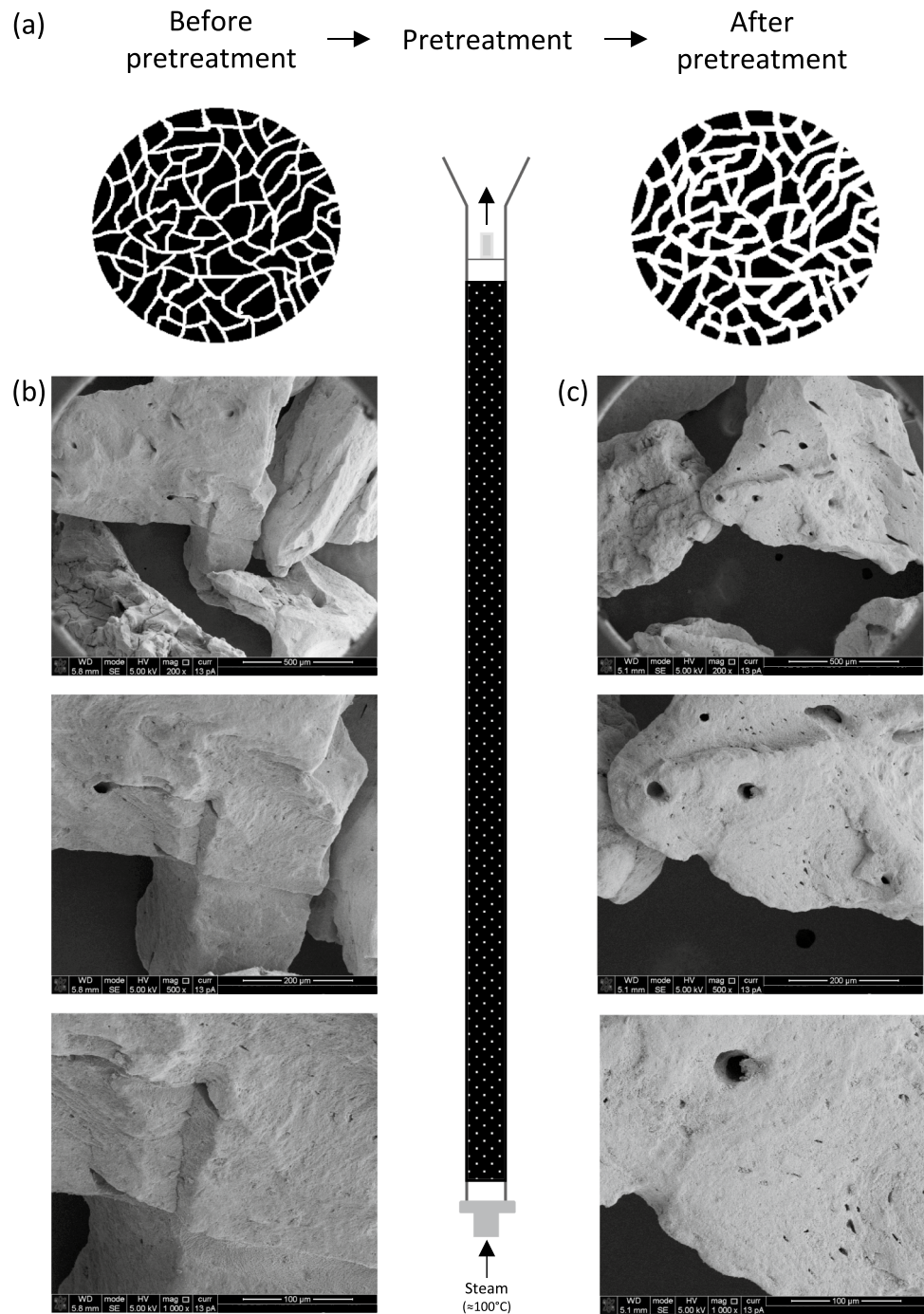
As expected, X-ray diffraction (XRD) confirmed the presence of crystalline structures of calcite (CaCO_3) in the bone char samples. According to Fig. 5, the hydroxyapatite was identified by peaks at approximately 2.80 Å (147 u.a. intensity for raw bone char and 162 u.a. for pretreated bone char), 1.94 Å (intensity of 46 u.a. for raw bone char and pretreated bone char), 3.45 Å (intensity of 61 u.a. for raw bone char and pretreated bone char), and 2.26 Å (intensity of 36 u.a. for raw bone char and 47 u.a. for pretreated bone char). The calcite was identified by peaks at approximately 3.09 Å (28 u.a. intensity for raw and pretreated bone char) and 1.45 Å (21 u.a. intensity for raw and pretreated bone char) (Rocha et al. 2012; Mesquita et al. 2017). The XRD analyses did not show significant changes in bone char samples after the pretreatment process. Few peaks could be distinguished by XRD analyses by raising the hypothesis of a general structure that tends to be amorphous. In fact, the hysteresis cycle obtained by N_2 adsorption–desorption analysis indicates that bone char could be composed of non-rigid aggregates of particles or that macropores, in the form of plates, of the

porous network, would not be completely filled, a fact also observed by Mesquita et al. (2017).

Figure 6 presents the results for raw and pretreated bone char PZC analysis. A pH_{PZC} of 6.81 ± 0.07 for raw bone char and of 6.70 ± 0.20 for pretreated bone char was estimated. Both bone char samples presented pH_{PZC} around the neutrality (7.00), which means that, in an alkaline environment, its surface charges will be negative and, otherwise, in an acid environment, its surface charges will be positive (Fagnani et al. 2017). As evidenced in Table 5, the pH of the effluent was higher than the pH_{PZC} , causing a negative surface in bone char that assists in the removal of phenolic compounds (Mushtaq et al. 2014). In this pH range and as the synthetic solution and effluent have pH around neutrality, the interaction of the phenolate ion with the fluid phase is greater than with the bone char surface because there is no excess of negative ions on the surface to the point of resulting in the repulsion of the phenolate ion (Guilarduci et al. 2006).

While the PCZ allows obtaining information about the interactions of the bone char surface with the medium, the evaluation of the interaction with a standard medium allows obtaining the pH of bone char due to protolytic processes occurring during the immersion of the samples (László et al. 2006). The pH values of the char suspension were 9.37 ± 0.05 and 8.96 ± 0.03 for raw and pretreated bone char, respectively. Thus, both adsorbents presented alkaline characteristics related to the carbonate presence, from a small amount of calcite (CaCO_3), a compound that confers the buffering property to the bone char (Mesquita et al. 2017). Coals with alkaline characteristics can adsorb more phenol molecules, which is this study's objective, for presenting a greater interaction between the basic groups of the surface with phenol (László et al. 2006). These groups are more present in larger pores, such as in larger micropores and mesopores, where this increase in

Fig. 4 **a** The effect of bone char pretreatment in surface area, total pore volume, and average pore diameter; **b** SEM images of bone char before pretreatment; **c** SEM images of bone char after pretreatment



concentration favors adsorption in those pores (Radovic et al. 2000).

Figure 7 shows the comparison of thermogravimetric analysis (TGA) of raw and pretreated bone char, which indicated, respectively, a total weight loss of 21.3 and 22.1% with the temperature increase from 30 up to 900 °C. The pretreated bone char mass loss was lower than the raw bone char up to 585 °C, where the pretreated bone char presented a greater mass loss.

Three regions of mass loss, for both, raw and pretreated bone char, were identified, as also observed by Ribeiro (2011) and Rojas-Mayorga et al. (2013). The first stage of mass loss, around 240 °C, corresponds to intrinsic and extrinsic water vaporization in the samples (Aziz et al. 2009; Lins et al. 2019). There was a weight loss of 6.1 and 5.5% for raw and pretreated bone char, respectively, in this stage. There was a difference in the final temperature between raw and pretreated bone char in the second region of mass loss. For raw bone char, it occurs between 240 and 595 °C,

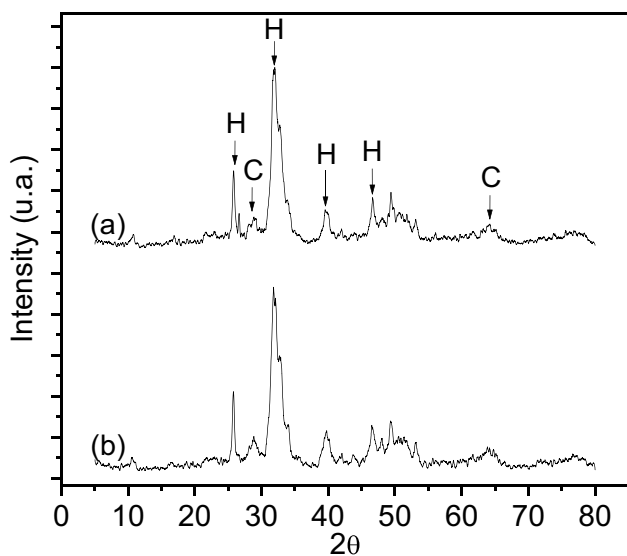


Fig. 5 Diffractograms of **a** raw and **b** pretreated bone char with calcite (C) peaks identified

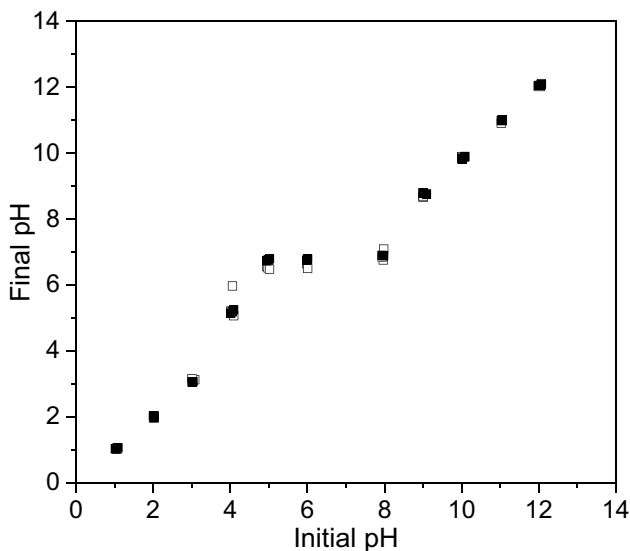


Fig. 6 Point of zero charge (PZC) determination of (■) raw (6.81 ± 0.07) and (□) pretreated bone char (6.70 ± 0.20)

with a weight loss of 12.2%, and for the pretreated, it occurs between 240 and 656 °C, with 14% of mass loss. This mass loss is related to the degradation of the organic carbon present in the bone char (Mesquita et al. 2018b). In the third region of mass loss, starting at 595 °C for raw and 656 °C for pretreated bone char and ending at 900 °C for both, there was a mass loss of 3.1% for raw and 2.6% for pretreated bone char. This stage is due to the decomposition of the carbonate, with CO₂ loss by calcite, which starts at 675 °C and can end in two different ways. The CO₂ loss by calcite can end with the complete degasification at 900 °C (Ribeiro

Table 5 EDR effluent characterization parameters

Parameters		EDR effluent
pH	–	7.30
Conductivity	[mS cm ⁻¹]	1.100
Bicarbonate alkalinity	[mg L ⁻¹]	216.67
Total alkalinity	[mg L ⁻¹]	216.67
Aluminum	[mg L ⁻¹]	< 1
Barium	[mg L ⁻¹]	< 1
Calcium	[mg L ⁻¹]	69.50
Chloride	[mg L ⁻¹]	619.81
COD	[mg L ⁻¹]	59.9
Strontium	[mg L ⁻¹]	4.67
Total Phosphorus	[mg L ⁻¹]	3.10
Magnesium	[mg L ⁻¹]	3.73
Potassium	[mg L ⁻¹]	10.40
Sodium	[mg L ⁻¹]	167.30
Sulfate	[mg L ⁻¹]	158.21
Total suspended solids	[mg L ⁻¹]	32.00
Turbidity	[NTU]	8.67

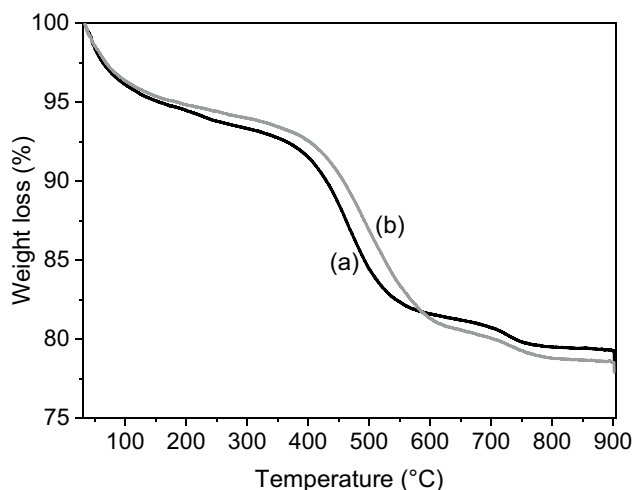


Fig. 7 Comparative thermogram of **a** raw and **b** steam pretreated bone char

2011) or with the dehydroxylation of hydroxyapatite, by the hydroxyl groups (–OH) loss and the consequent loss of the lamellar structure, which occurs between 600 and 800 °C (Patel et al. 2015; Mesquita et al. 2017). Differences in the thermogravimetric analysis at temperatures above 100 °C (the temperature used in the pretreatment) were not expected and may indicate possible removals of less volatile fractions by physical forms (such as drag) that are outside the scope of this work.

The Fourier transformed infrared spectroscopy (FTIR) spectra obtained for raw and pretreated bone char were similar (Fig. 8), just with less intense spectra bands for the

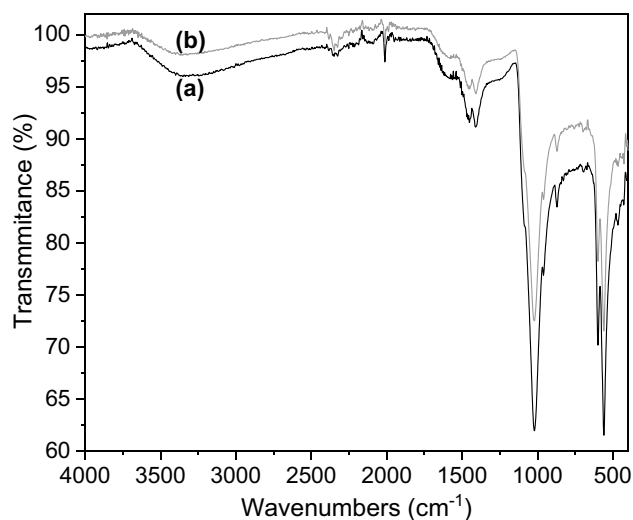


Fig. 8 FTIR spectra analysis for **a** raw and **b** pretreated bone char

pretreated bone char. At all wavelengths, the percentage transmittance showed a decrease in the bonds of functional groups in the pretreated bone char (Rezaee et al. 2013). The bands with the highest (1461 cm^{-1}) and lowest (871 cm^{-1}) intensity were attributed to carbonate groups (CO_3^{2-}). The bands between 560 and 600 cm^{-1} and between 1000 and 1100 cm^{-1} were assigned to phosphate groups (PO_4^{3-}). The wide band, between 2600 and 3600 cm^{-1} , is due to the hydroxyl groups ($-\text{OH}$), present in hydroxyapatite and typical in bone char samples (Boukha et al. 2007; Berzina-Cimdina and Borodajenko 2012; Mesquita et al. 2017).

The steam pretreatment provided a greater surface area and porosity to the pretreated bone char in comparison to raw bone char. It is possible that the steam pretreatment also removed impurities adhered to the bone char, favoring the adsorbate physisorption. Major structural changes have not been observed and the mechanism involving pretreatment with steam at $100\text{ }^\circ\text{C}$ cannot be fully elucidated. Thus, adsorption tests were performed seeking to understand the gain that this pretreatment provides to the adsorption process of refractory compounds, mainly phenolic compounds.

EDR effluent characterization

Table 5 shows the results of the EDR effluent characterization. The EDR effluent presented a pH close to neutrality, equal to 7.3 ± 0.1 . The low turbidity of 8.7 ± 0.2 NTU may be related to a low value of total suspended solids. The refractory organics concentration, in terms of chemical oxygen demand (COD), was $59.9 \pm 1.6\text{ mg L}^{-1}$. The concentration of COD is similar to that found by Machado (2008), which defines it as about 60 mg L^{-1} . This COD value was used as a reference for the synthetic solution of phenol. In a study by Mesquita et al. (2017), close to

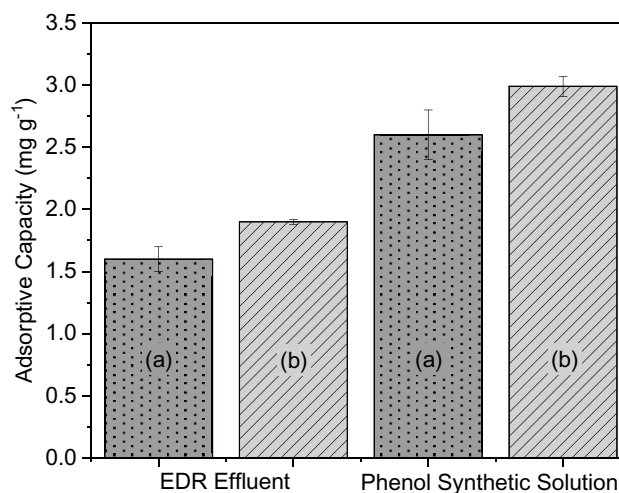


Fig. 9 Adsorptive capacities of **a** raw and **b** pretreated bone char for removal of refractory organics and phenol in the batch system

70 substances can be identified by chromatography, where many were phenolic compounds.

Alkalinity is the number of ions in the water that will react to neutralize H^+ ions, it is a measurement of the water's ability to neutralize acids (ability to resist pH changes: buffering capacity). The main constituents of alkalinity are bicarbonates, carbonates, and hydroxides. The distribution between the three forms depends on the pH. As the pH is close to neutrality, it has been that alkalinity is mainly due to bicarbonate, as shown in Table 4. Conductivity and ions were much lower in the effluent of this work and below that defined for direct reuse purposes ($1.400\text{--}1.900\text{ }\mu\text{S/cm}$) (Pombo et al. 2011). However, the concentration is still high and identifies the effluent as saline. It should be noted that the characteristics of effluent may vary significantly depending on the process conditions on the day of collection.

Batch adsorption experiments

The results of adsorptive capacity (q_0) obtained in batch tests to evaluate the removal of refractory organics from EDR effluent and phenol from synthetic solution by raw and pretreated bone chars are shown in Fig. 9.

For both raw and pretreated char, the removal of organic compounds, in terms of COD, was higher from the phenol synthetic solution compared to the EDR effluent. This happens because of the difference in composition of both fluid phases. The other compounds present in EDR effluent, besides phenolic ones, may have been adsorbed before the phenol, some because are smaller molecules, others due to having more affinity with the adsorbent surface (Souza et al. 2012).

Figure 9 shows that, for both effluents, the adsorptive capacities are higher using the pretreated bone char. For the

EDR effluent, the adsorptive capacities were 1.62 ± 0.11 and 1.92 ± 0.02 mg g⁻¹ for raw and pretreated bone char, respectively. For the phenol synthetic solution, the adsorptive capacities were 2.60 ± 0.09 and 2.99 ± 0.08 mg g⁻¹ for raw and pretreated bone char, respectively.

Due to the better performance of the pretreated bone char, with adsorption capacity around 0.30 mg g⁻¹ or 19% higher for the EDR effluent and 0.39 mg g⁻¹ or 15% higher for the phenol synthetic solution, it is believed that the bone char pretreatment effects evidenced in the characterization stage, as an increase in surface area, total pore volume, and average pore diameter, ensured better performance. The use of steam with temperatures of 100 °C in pretreatments was not observed in recent literature but showed a gain when used with bone char. In addition, it was observed that the bone char pretreatment favored a greater increase in the adsorptive capacity of the EDR effluent. This was associated with the presence of complex phenolic compounds with larger carbon chains, which were possible to be removed with the increase of the pore diameter (Mesquita et al. 2017).

The adsorption mechanism of the refractory organic compounds by bone char was previously studied through batch tests by Mesquita et al. (2018b), and there is no evidence that major changes occurred with steam pretreatment. The authors reported physisorption and uncovered the formation of multilayers and rapid initial adsorption that suggested the occupation of active sites by larger molecules. As these sites became saturated, the diffusion of the solute into the adsorbent's pores slowed down. Consequently, a subsequent layer of adsorption is initiated, perpetuating the process.

In any case, bone char (BC) seems to be a good adsorbent for phenolic compounds and steam pretreatment has proven to be a potential method to improve its adsorption capacity. Although bone char surface area is much smaller compared to conventional activated carbons (AC), better long-chain refractory organics removal performance from saline concentrate wastewater when using bovine bone char, compared to the conventional AC tested (up to 15% better), was reported by Mesquita (2016). This may be explained by the different porous matrix (predominantly mesoporous BC x predominantly microporous AC), and also by BC larger micropores average diameter. These characteristics favored the access of long-chain organic molecules to active sites. Indeed, the author highlights “the hypothesis of steric hindrance for penetration into the micropores due to the size of the adsorbate molecules (long-chain hydrocarbons). In other words, part of the adsorptive capacity is compromised by the adsorptive process that occurs inside the adsorbent pores.”

Another point to ponder is that bone chars are distinguished from other available adsorbents because they contain around 80–90% hydroxyapatite (HAP) and only

around 10% by mass of amorphous carbon (Patel et al. 2015; Azeem et al. 2022; Piccirillo 2023). This is contrary to what is observed in the usual adsorbents, such as activated carbons (Huang et al. 2022; Amalina et al. 2022; Medellín Castillo et al. 2023). HAP has the ability to replace cations and anions and also has a high capacity to bind to organic molecules of different sizes (Patel et al. 2015; Piccirillo et al. 2017; Medellín Castillo et al. 2023). In addition to having good sorption efficiency, HAP is highly stable under oxidation–reduction conditions and has good buffering capacity (Nigri et al. 2017a; Piccirillo et al. 2017; Alkurdi et al. 2020).

Also, for adsorption to be efficient and economically satisfactory, several other factors must be considered, such as the adsorbent cost and use limitation. A loss of performance due to salinity (which was the case in the wastewater investigated) while using conventional AC is reported. The high cost associated with commercial activated carbon is also a relevant factor when thinking about scalability for larger treatment applications (Mesquita et al. 2017; Mesquita et al. 2018b). Geça et al. (2022) presented a comparison of alternative adsorbents and activated carbons for the removal of organic compounds from multicomponent systems. The alternative adsorbents, such as the bone char, offered a favorable cost-effectiveness relationship, making them suitable for real wastewater treatment systems. Furthermore, the use of alternative adsorbents replacing commercial activated carbon is more than simply exchanging products based on cost or efficiency. This may represent the possibility of appropriate disposal of waste from other activities, such as the bovine bones. In addition to adsorption as an efficient wastewater treatment technique, the production and application of alternative adsorbents can be seen as a positive environmental contribution to solid waste management.

Fixed bed adsorption experiments

The breakthrough curve obtained for the phenol removal test by adsorption in a pretreated bone char fixed-bed column is shown in Fig. 10. The obtained breakthrough curve presents the sigmoidal format pattern of the breakthrough curves in the literature and suggests its beginning in relative concentration values (C/C_0) close to zero and its stabilization close to 1. The adsorptive capacity (q_0) calculated from the breakthrough curve and the operational conditions of the semi-continuous test with pretreated bone char for phenol removal was 2.88 mg.g⁻¹ ($R^2 = 0.9884$). Comparing to the results of the batch tests with pretreated bone char for phenol removal ($q_0 = 2.99 \pm 0.08$ mg.g⁻¹), the value obtained in a semi-continuous system corroborates with a removal ratio of about 3:1 mg of phenol per gram of steam-pretreated bone char.

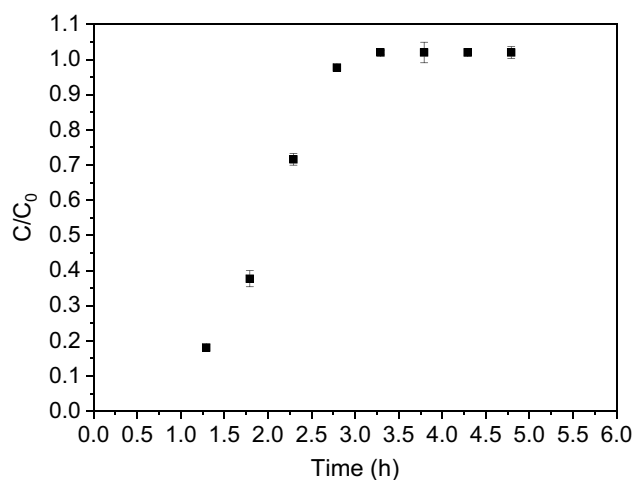


Fig. 10 Breakthrough curve of phenol adsorption by pretreated bone char in a fixed-bed column, in terms of relative concentration (C/C_0)

The operational and dynamic parameters, which describe the behavior of the breakthrough curve and the dynamic of phenol adsorption by pretreated bone char in a fixed-bed column are shown in Table 6. The bed volume ($V_R = 210$ mL) reflects the amount of adsorbent available in the column, and it is directly related to the availability of surface area and active sites for adsorption (Kizito et al. 2016; Ebrahiem et al. 2018; Dawood et al. 2019). The visibility of the breakthrough point (Fig. 10) suggests that the column operated with a sufficient number of adsorbent particles ($Z_A = 3941$) and met the phenol removal need (Cavalcanti 2016; Nigri et al. 2017b; Mesquita et al. 2018b).

Due to the low value of bed porosity of 16%, the column cross-sectional area (A_S) available for the fluid phase passage was significantly reduced by the adsorbent presence, expressed by the bed volume filled by the adsorbent mass ($V_A = 1.77$ mL) (Worch 2012; Mesquita et al. 2018b). Therefore, the effective fluid phase velocity ($Q_E = 8.44$ cm. min^{-1}) calculated is 6 times higher than the fluid phase superficial velocity (Q_S) equal to 1.33 cm. min^{-1} . Also due to the bed porosity (ϵ_R), the empty bed contact time (EBTC = 4.10 min) is reduced to the effective fluid phase residence time ($t_R = 0.65$ min), an 84% reduction. In addition to the bed porosity (ϵ_R), the empty bed contact time (EBCT) is also related to the volumetric flow, in terms of fluid phase superficial velocity (Q_S). Among the operational parameters that interfere in the efficiency of the adsorption process is the contact time between adsorbate and adsorbent. It is indispensable that the empty bed contact time (EBTC) is large enough for effective interaction between adsorbate and adsorbent and, consequently, for the adsorption to occur (Worch 2012; Cavalcanti 2016; Mesquita et al. 2018b).

The adsorption process efficiency (η) was 50.7% for phenol removal onto pretreated bone char. In other words, in addition to retaining about 2.88 mg of adsorbate per gram of adsorbent, under these operational conditions, the system reached an adsorptive capacity up to the breakthrough point (q_B) equivalent to half of the total adsorptive capacity (q_0). So, half of the system's total capacity occurs in meeting the removal needs, before achieving the breakthrough time ($t_B = 59.4$ min) (Worch 2012).

The mass transfer resistance directly affects the bed length used up to the breakthrough point, expressed as the

Table 6 Operational and dynamic parameters of phenol adsorption by pretreated bone char in a fixed-bed column

Parameters			Values	
Operational	Bed volume	V_R [mL]	2.10	
	Bed volume filled by the adsorbent mass	V_A [mL]	1.77	
	Empty bed volume	V_L [mL]	0.33	
	Bed density	ρ_R [g cm^{-3}]	0.57	
	Bed porosity	ϵ_R [%]	16	
	Bed adsorbent particle number	Z_A	3941	
	Fluid phase superficial velocity	Q_S [cm min^{-1}]	1.33	
	Effective fluid phase velocity	Q_E [cm min^{-1}]	8.44	
	Empty bed contact time	EBTC [min]	4.10	
	Effective fluid phase residence time	t_R [min]	0.65	
	Dynamic	Process efficiency	η [%]	50.7
		Effective bed use	h_E [cm]	2.8
		Length of unused bed	LUB [cm]	2.7
Mass transfer zone movement time		t_M [h]	1.83	
Fractional adsorbent capacity		F	0.50	
Mass transfer zone formation time		t_F [h]	0.91	
Mass transfer zone height		h_Z [cm]	5.2	
Mass transfer zone movement rate	U_Z [cm h^{-1}]	2.87		

effective bed use (h_E) (Worch 2012; Nigri et al. 2017b; Mesquita et al. 2018b). In this work, the effective bed use (h_E) was close to the length of the unused bed (LUB), 2.8 and 2.7 cm, respectively. Thus, it can be suggested that the system was operated at an intermediate volumetric flow rate (Q), with consequent median resistance of mass transfer. Thus, about 51% of the total bed length was used before the breakthrough point, meeting the need for adsorbate removal.

Evaluating the other dynamic parameters, the height (h_Z) and the movement time (t_M) of the mass transfer zone (MTZ) are also associated with the mass transfer resistance, which in turn is related to the volumetric flow rate (Q). For the operational conditions used in the phenol/pretreated bone

char semi-continuous system, the MTZ height (h_Z) is equal to 5.2 cm, almost the bed depth (h) value of 5.5 cm, pointing at a relatively high slope of the breakthrough curve. Higher slopes are directly related to lower mass transfer resistances and higher volumetric flow rates (Q) (Worch 2012; Nigri et al. 2017b; Mesquita et al. 2018b). Finally, the elevated MTZ height (h_Z) takes to a low MTZ movement time ($t_M = 1.83$ h) and, consequently, a high MTZ movement rate ($U_Z = 2.87$ cm h⁻¹).

Thus, the slope of the breakthrough curve and the dynamic parameters obtained suggest that the semi-continuous test was performed using an intermediate to high volumetric flow rate (Q), favorable to the adsorption due to the mass transfer resistance reduction.

Figure 11 shows the experimental and predicted breakthrough curves obtained by Thomas, Yoon and Nelson, and Yan fit the experimental breakthrough curve. The adsorptive capacity and parameters obtained by mathematical modeling are shown in Table 7.

From Fig. 11, it is noted that among the models evaluated, the models by Thomas, Yoon and Nelson, and Yan presented a satisfactory fit to the experimental breakthrough curve. However, high values of R^2 and low values of %D and AIC_C pointed to the models of Thomas and Yoon model and Nelson model as the best ones to describe experimental data, as shown in Table 7. The proximity between the values of experimental adsorptive capacity ($q_0 = 2.88$ mg g⁻¹) and adsorptive capacity predicted by Thomas's model ($q_T = 2.90$ mg g⁻¹) corroborates its satisfactory fit. The fit of the Wolborska model to the experimental data was not adequate and was suppressed from the results since low

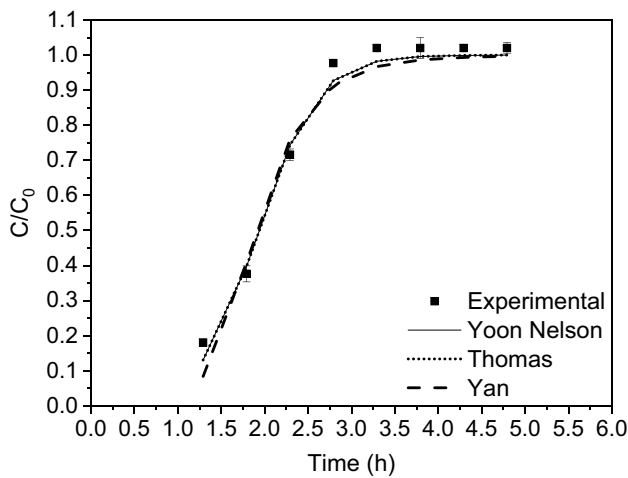


Fig. 11 Experimental and predicted breakthrough curves by Thomas, Yoon and Nelson, and Yan models

Table 7 Parameters obtained from mathematical modeling

Models	Parameters	Values	
Thomas	Adsorptive capacity	q_T [mg g ⁻¹]	2.90
	Thomas rate constant	K_T [L mg ⁻¹ h ⁻¹]	0.05
	Determination coefficient	R^2	0.9836
	Average absolute deviation	%D	6.76
	Corrected Akaike information criteria	AIC_C	-39.29
Yoon and Nelson	Time required to reach $C/C_0=0.5$	τ [h]	1.93
	Yoon and Nelson constant	K_{YN} [h ⁻¹]	2.96
	Determination coefficient	R^2	0.9836
	Average absolute deviation	%D	6.76
	Corrected Akaike information criteria	AIC_C	-39.29
Yan	Adsorptive capacity	q_Y [mg g ⁻¹]	2.85
	Yan constant model	a_Y	6.16
	Determination coefficient	R^2	0.9671
	Average absolute deviation	%D	11.13
	Corrected Akaike information criteria	AIC_C	-33.69
Experimental	Adsorptive capacity	q_0 [mg g ⁻¹]	2.88
	Determination coefficient	R^2	0.9884

values of R^2 (0.6165) and high values of %D (39.13) and AIC_C (−14.06) were obtained.

In Fig. 11, it is noted an overlap of the breakthrough curves predicted by Thomas and Yoon and Nelson models. In Table 7, such overlap is confirmed by identical values of R^2 , %D, and AIC_C . Thomas and Yoon model and Nelson model are mathematically equivalent, differing only in the physical meaning of their parameters and in the amount of data needed to adjust them. Thus, the observed overlap was expected (Thomas 1944; Xu et al. 2013; Santos et al. 2020).

Conclusions

The characterization of raw and pretreated bone char suggested an increase in bone char surface area and porosity due to the pretreatment. It is possible that the steam pretreatment also removed impurities adhered to the bone char, favoring the adsorbate physisorption. Major structural changes have not been observed and the mechanism involving pretreatment with steam at 100 °C could not be fully elucidated. Better performance of steam-treated bone char, in both modes, batch and semi-continuous, was attained, compared to the raw bone char. The adsorptive capacities of the pretreated bone char were around 15% higher for phenol removal from synthetic solution and 19% higher for refractory organics removal from EDR effluent in batch tests.

The semi-continuous system operated in a fixed-bed for phenol removal from synthetic solution showed adsorptive capacity close to the obtained in the batch tests, with values of 2.88 and 2.99 mg g^{−1}, respectively. The breakthrough curve presented a sigmoidal format pattern, and the adsorption process efficiency was 50.7%. The test was performed using an intermediate-to-high volumetric flow rate, favorable to the adsorption due to the mass transfer resistance reduction. Thomas ($R^2 = 0.9836$) and Yoon and Nelson ($R^2 = 0.9836$) models were the best to describe breakthrough curve experimental data, with low average absolute deviations (around 6%).

Acknowledgements The authors acknowledge CAPES (Coordenação de Aperfeiçoamento de Pessoal de Nível Superior—Brazilian Higher Education Personnel Improvement Coordination, Finance Code 01), PPGEQ/UFSJ (Post Graduate Program in Chemical Engineering/Federal University of São João del-Rei), Laboratório de Processamento Mineral e Meio Ambiente (Federal University of Minas Gerais/Brazil), Laboratório de Caracterização de Minérios e Materiais (Federal University of Minas Gerais/Brazil), and Bonechar Carvão Ativado do Brasil.

Author contributions All authors contributed to the conception and design of the study. Material preparation, data collection, and laboratory analysis were performed by FdAL, IPdS, and PVdOV. All authors contributed to data analysis, discussion of the manuscript results, and writing.

Funding This work was supported by the UFSJ (Federal University of São João del-Rei) and CAPES (Coordenação de Aperfeiçoamento de Pessoal de Nível Superior—Brazilian Higher Education Personnel Improvement Coordination, Finance Code 01).

Data availability The data used in this study can be provided by the corresponding author upon reasonable request.

Declarations

Conflict of interest The authors declare no competing interests.

Ethical approval Not applicable.

Consent to participate Not applicable.

Consent for publication Not applicable.

References

- Abbassian K, Kargari A, Kaghazchi T (2015) Phenol removal from aqueous solutions by a novel industrial solvent. *Chem Eng Commun* 202(3):408–413. <https://doi.org/10.1080/00986445.2013.848804>
- ABNT (1991) NBR 12076/1991 - Carvão ativado pulverizado: Determinação da massa específica aparente. Assoc Bras Normas Técnicas, Rio de Janeiro
- ABNT (2001) NBR NM 27/2001 - Agregados - Redução da amostra de campo para ensaios de laboratório. Assoc Bras Normas Técnicas, Rio de Janeiro
- ABNT (2017) NBR 16586/2017 - Método de ensaio para determinação do teor de cinzas. Assoc Bras Normas Técnicas, Rio de Janeiro
- Adamiak K (2013) Numerical models in simulating wire-plate electrostatic precipitators: a review. *J Electrostat* 71(4):673–680. <https://doi.org/10.1016/j.elstat.2013.03.001>
- Alkurdi SSA, Al-Juboori RA, Bundschuh J, Bowtell L, McKnight S (2020) Effect of pyrolysis conditions on bone char characterization and its ability for arsenic and fluoride removal. *Environ Pollut* 262:114221. <https://doi.org/10.1016/j.envpol.2020.114221>
- Alva-Argáez A, Kokossis AC, Smith R (2007) The design of water-using systems in petroleum refining using a water-pinch decomposition. *Chem Eng J* 128(1):33–46. <https://doi.org/10.1016/j.cej.2006.10.001>
- Amalina F, Syukor Abd Razak A, Krishnan S, Sulaiman H, Zularisam AW, Nasrullah M (2022) Advanced techniques in the production of biochar from lignocellulosic biomass and environmental applications. *Clean Mater* 6:100137. <https://doi.org/10.1016/j.clema.2022.100137>
- APHA (2017) Standard methods for the examination of water and wastewater. American Public Health, Washington DC
- Azeem M, Shaheen SM, Ali A, Jeyasundar PGSA, Latif A, Abdelrahman H, Li R, Almazroui M, Niazi NK, Sarmah AK, Li G, Rinklebe J, Zhu Y-G, Zhang Z (2022) Removal of potentially toxic elements from contaminated soil and water using bone char compared to plant- and bone-derived biochars: a review. *J Hazard Mater* 427:128131. <https://doi.org/10.1016/j.jhazmat.2021.128131>
- Aziz A, Elandaloussi EH, Belhafaoui B, Ouali MS, De Ménorval LC (2009) Efficiency of succinylated-olive stone biosorbent on the removal of cadmium ions from aqueous solutions. *Colloids Surf B Biointerfaces* 73(2):192–198. <https://doi.org/10.1016/j.colsurfb.2009.05.017>

- Becheleni EMA, Borba RP, Seckler MM, Rocha SDF (2015) Water recovery from saline streams produced by electro dialysis. *Environ Technol* 36(3):386–394. <https://doi.org/10.1080/09593330.2014.978898>
- Becheleni EMA, Rodriguez-Pascual M, Lewis AE, Rocha SDF (2017) Influence of phenol on the crystallization kinetics and quality of ice and sodium sulfate decahydrate during eutectic freeze crystallization. *Ind Eng Chem Res* 56(41):11926–11935. <https://doi.org/10.1021/acs.iecr.7b02668>
- Berzina-Cimdina L, Borodajenko N (2012) Research of calcium phosphates using Fourier transform infrared spectroscopy. Infrared spectroscopy—materials science, engineering and technology. InTech, pp 251–263
- Bonate PL (2011) Pharmacokinetic-pharmacodynamic modeling and simulation. Springer US, Boston
- BONECHAR (2018) Carvão Ativado. <http://www.bonechar.com.br/carvao-ativado>. Accessed 18 May 2018
- Boukha Z, Kacimi M, Pereira MFR, Faria JL, Figueiredo JL, Ziyad M (2007) Methane dry reforming on Ni loaded hydroxyapatite and fluoroapatite. *Appl Catal A Gen* 317(2):299–309. <https://doi.org/10.1016/j.apcata.2006.10.029>
- Brunson LR, Sabatini DA (2014) Practical considerations, column studies and natural organic material competition for fluoride removal with bone char and aluminum amended materials in the Main Ethiopian Rift Valley. *Sci Total Environ* 488–489:580–587. <https://doi.org/10.1016/j.scitotenv.2013.12.048>
- Cavalcanti J (2016) Manual de tratamento de efluentes industriais, 3rd edn. Engenho Editora Técnica, São Paulo
- Cazetta AL, Azevedo SP, Pezoti O, Souza LS, Vargas AMM, Paulino AT, Moraes JCG, Almeida VC (2014) Thermally activated carbon from bovine bone: optimization of synthesis conditions by response surface methodology. *J Anal Appl Pyrolysis* 110:455–462. <https://doi.org/10.1016/j.jaap.2014.10.022>
- Choi J-S, Kim J-T (2015) Modeling of full-scale reverse osmosis desalination system: influence of operational parameters. *J Ind Eng Chem* 21:261–268
- Chong TH, Loo S-L, Krantz WB (2015) Energy-efficient reverse osmosis desalination process. *J Memb Sci* 473:177–188
- Coltre DS, Cionek CA, Meneguín JG, Maeda CH, Braga MU, de Araújo AC, Gauze GD, de Barros MA, Arroyo PA (2020) Study of dye desorption mechanism of bone char utilizing different regenerating agents. *SN Appl Sci* 2(12):2150. <https://doi.org/10.1007/s42452-020-03911-8>
- Cristóvão RO, Botelho CM, Martins RJE, Loureiro JM, Boaventura RAR (2015) Fish canning industry wastewater treatment for water reuse—a case study. *J Clean Prod* 87:603–612
- Cruz MAP, Guimarães LCM, da Costa Júnior EF, Rocha SDF, da Mesquita PL (2020) Adsorption of crystal violet from aqueous solution in continuous flow system using bone char. *Chem Eng Commun* 207(3):372–381. <https://doi.org/10.1080/00986445.2019.1596899>
- Dawood S, Sen TK, Phan C (2019) Performance and dynamic modelling of biochar and kaolin packed bed adsorption column for aqueous phase methylene blue (MB) dye removal. *Environ Technol* 40(28):3762–3772. <https://doi.org/10.1080/09593330.2018.1491065>
- Domingos RA, Fonseca FV (2018) Evaluation of adsorbent and ion exchange resins for removal of organic matter from petroleum refinery wastewaters aiming to increase water reuse. *J Environ Manag* 214:362–369. <https://doi.org/10.1016/j.jenvman.2018.03.022>
- Ebrahimi EE, Altaher H, Abdelghany EA, Magdy YH (2018) Packed bed column for adsorption of aqueous phenols on cement kiln dust. *J Hazard Toxic, Radioact Waste* 22(3):04018009. [https://doi.org/10.1061/\(ASCE\)HZ.2153-5515.0000401](https://doi.org/10.1061/(ASCE)HZ.2153-5515.0000401)
- Fagnani HMC, Deolin ME, de Barros MASD, Arroyo PA (2017) Identificação dos mecanismos de sorção em zeólita NaY e sílica gel. *Matéria* 22(3):200. <https://doi.org/10.1590/s1517-707620170003.0195>
- Gangupomu RH, Sattler ML, Ramirez D (2016) Comparative study of carbon nanotubes and granular activated carbon: physico-chemical properties and adsorption capacities. *J Hazard Mater* 302:362–374. <https://doi.org/10.1016/j.jhazmat.2015.09.002>
- Geça M, Wiśniewska M, Nowicki P (2022) Biochars and activated carbons as adsorbents of inorganic and organic compounds from multicomponent systems—A review. *Adv Colloid Interface Sci* 305:102687. <https://doi.org/10.1016/j.cis.2022.102687>
- Ghanizadeh G, Asgari G (2011) Adsorption kinetics and isotherm of methylene blue and its removal from aqueous solution using bone charcoal. *React Kinet Mech Catal* 102(1):127–142. <https://doi.org/10.1007/s11144-010-0247-2>
- Guilarduci VV, Mesquita JP, Martelli PB, Gorgulho HD (2006) Adsorção de fenol sobre carvão ativado em meio alcalino. *Quim Nova* 29:1226–1232. <https://doi.org/10.1590/S0100-40422006000600015>
- Harrison RG, Todd P, Rudge SR, Petrides DP (2015) Bioseparations science and engineering. Topics in chemical engineering, 2nd edn. Oxford University Press, New York
- Hart A, Porbeni DW, Omonmhenle S, Peretomode E (2023) Waste bone char-derived adsorbents: characteristics, adsorption mechanism and model approach. *Environ Technol Rev* 12(1):175–204. <https://doi.org/10.1080/21622515.2023.2197128>
- Hashemi S, Rezaee A, Nikodel M, Ganjidost H, Mousavi SM (2013) Equilibrium and kinetic studies of the adsorption of sodium dodecyl sulfate from aqueous solution using bone char. *React Kinet Mech Catal* 109(2):433–446. <https://doi.org/10.1007/s11144-013-0559-0>
- He X, Wang L, Lau A (2020) Investigation of steam treatment on the sorption behavior of rice straw pellets. *Energies* 13(20):5401. <https://doi.org/10.3390/en13205401>
- Huang L, Luo Z, Huang X, Wang Y, Yan J, Liu W, Guo Y, Babu Arulmani SR, Shao M, Zhang H (2022) Applications of biomass-based materials to remove fluoride from wastewater: a review. *Chemosphere* 301:134679. <https://doi.org/10.1016/j.chemosphere.2022.134679>
- Kennedy AM, Arias-Paic M (2020) Fixed-bed adsorption comparisons of bone char and activated alumina for the removal of fluoride from drinking water. *J Environ Eng. (ASCE)* EE.1943-7870.0001625
- Kizito S, Wu S, Wandera SM, Guo L, Dong R (2016) Evaluation of ammonium adsorption in biochar-fixed beds for treatment of anaerobically digested swine slurry: experimental optimization and modeling. *Sci Total Environ* 563–564:1095–1104. <https://doi.org/10.1016/j.scitotenv.2016.05.149>
- László K, Podkościelny P, Dąbrowski A (2006) Heterogeneity of activated carbons with different surface chemistry in adsorption of phenol from aqueous solutions. *Appl Surf Sci* 252(16):5752–5762. <https://doi.org/10.1016/j.apsusc.2005.07.027>
- Lebigue CJ, Andriantsiferana C, Krou N, Ayrat C, Mohamed E, Wilhelm A-M, Delmas H, Le Coq L, Gerente C, Smith KM, Pullket S, Fowler GD, Graham NJD (2010) Application of sludge-based carbonaceous materials in a hybrid water treatment process based on adsorption and catalytic wet air oxidation. *J Environ Manag* 91(12):2432–2439. <https://doi.org/10.1016/j.jenvman.2010.06.008>
- Li D, Sun T, Wang L, Wang N (2018) Enhanced electro-catalytic generation of hydrogen peroxide and hydroxyl radical for degradation of phenol wastewater using MnO₂/Nano-GlFoam-Ni/Pd composite cathode. *Electrochim Acta* 282:416–426. <https://doi.org/10.1016/j.electacta.2018.06.075>

- Li N, He M, Lu X, Yan B, Duan X, Chen G, Wang S, Hou L (2022) Municipal solid waste derived biochars for wastewater treatment: production, properties and applications. *Resour Conserv Recycl* 177:106003. <https://doi.org/10.1016/j.resconrec.2021.106003>
- Li Z-Y, Akhtar MS, Kwak D-H, Yang O-B (2017) Improvement in the surface properties of activated carbon via steam pretreatment for high performance supercapacitors. *Appl Surf Sci* 404:88–93. <https://doi.org/10.1016/j.apsusc.2017.01.238>
- Santos Lins PV, Henrique DC, Ide AH, Zanta CLPS, Meili L (2019) Evaluation of caffeine adsorption by MgAl-LDH/biochar composite. *Environ Sci Pollut Res* 26:31804–31811. <https://doi.org/10.1007/s11356-019-06288-3>
- Liu K, Li F, Tian Q, Nie C, Ma Y, Zhu Z, Fang L, Huang Y, Liu S (2021) A highly porous animal bone-derived char with a superiority of promoting nZVI for Cr(VI) sequestration in agricultural soils. *J Environ Sci* 104:27–39. <https://doi.org/10.1016/j.jes.2020.11.031>
- Machado MB (2008) Avaliação do processo de eletrodialise reversa no tratamento de efluentes de refinaria de petróleo. Federal University of Rio Grande do Sul
- Maeng M-S, Byun J-S, Park H-J, Shin G-A (2020) Optimum operating conditions of drinking water treatment system for fluoride removal using high adsorption bone char. *J Korean Soc Environ Eng* 42(11):520–528. <https://doi.org/10.4491/KSEE.2020.42.11.520>
- Maria ME, Mansur MB (2017) Mathematical modeling of manganese adsorption onto bone char in a continuous fixed bed column incorporating backmixing and shrinking core approaches. *Braz J Chem Eng* 34(3):901–909. <https://doi.org/10.1590/0104-6632.20170343s20150625>
- Medellín Castillo NA, González Fernández LA, Thiodjio-Sendja B, Aguilera-Flores MM, Leyva-Ramos R, Reyes-López SY, de León-Martínez LD, Dias JM (2023) Bone char for water treatment and environmental applications: a review. *J Anal Appl Pyrolysis* 175:106161. <https://doi.org/10.1016/j.jaap.2023.106161>
- Mesquita PL (2016) Uso de carvão de ossos bovinos na remoção de contaminantes orgânicos de concentrados de eletrodialise e sua contribuição ao reuso de água na indústria de petróleo. Federal University of Minas Gerais
- Mesquita PD, Cruz MA, Souza CR, Santos NT, Nucci ER, Rocha SD (2017) Removal of refractory organics from saline concentrate produced by electro dialysis in petroleum industry using bone char. *Adsorption* 23:983–997. <https://doi.org/10.1007/s10450-017-9917-y>
- Mesquita PL, Mihara HY, Rocha SD (2018a) Regeneração a vapor de carvão de ossos bovinos usado como adsorvente para remoção de orgânicos refratários de concentrado salino do tratamento de efluentes da indústria de petróleo. In: Encontro Brasileiro de Adsorçã. Gramado, Brasil, pp 23–25
- Mesquita PD, Souza CR, Santos NT, Rocha SD (2018b) Fixed-bed study for bone char adsorptive removal of refractory organics from electro dialysis concentrate produced by petroleum refinery. *Environ Technol* 39:1544–1556. <https://doi.org/10.1080/0959330.2017.1332691>
- Metcalf L, Eddy HP, Burton FL, Stensel HD, Tchobanoglous G (2014) Wastewater engineering: treatment and reuse, 5th edn. McGraw-Hill Education, Boston
- Moreno JC, Gómez R, Giraldo L (2010) Removal of Mn, Fe, Ni and Cu ions from wastewater using cow bone charcoal. *Materials* 3(1):452–466. <https://doi.org/10.3390/ma3010452>
- Moussavi SP, Kadier A, Singh R, Ashoori R, Shirinkar M, Lu J, Zaidi NS, Sher F (2022) Superior removal of humic acid from aqueous stream using novel calf bones charcoal nano adsorbent in a reversible process. *Chemosphere* 301:134673. <https://doi.org/10.1016/j.chemosphere.2022.134673>
- Mushtaq M, Tan IM, Ismail L, Nadeem M, Sagir M, Azam R, Hashmet R (2014) Influence of PZC (point of zero charge) on the static adsorption of anionic surfactants on a Malaysian sandstone. *J Dispers Sci Technol* 35(3):343–349. <https://doi.org/10.1080/01932691.2013.785362>
- Nascimento RF, Lima AC, Vidal CB, Melo DD, Raulino GS (2014) Adsorção: aspectos teóricos e aplicações ambientais. Imprensa Universitária, Fortaleza
- Nascimento PFP, Barros Neto EL (2021) Steam explosion: hydrothermal pretreatment in the production of an adsorbent material using coconut husk. *BioEnergy Res* 14(1):153–162. <https://doi.org/10.1007/s12155-020-10159-y>
- Nigri EM, Bhatnagar A, Rocha SDF (2017a) Thermal regeneration process of bone char used in the fluoride removal from aqueous solution. *J Clean Prod* 142:3558–3570. <https://doi.org/10.1016/j.jclepro.2016.10.112>
- Nigri EM, Cechinel MAP, Mayer DA, Mazur LP, Loureiro JM, Rocha SDF, Vilar VJP (2017b) Cow bones char as a green sorbent for fluorides removal from aqueous solutions: batch and fixed-bed studies. *Environ Sci Pollut Res* 24(3):2364–2380. <https://doi.org/10.1007/s11356-016-7816-5>
- Panigrahy N, Priyadarshini A, Sahoo MM, Verma AK, Daverey A, Sahoo NK (2022) A comprehensive review on eco-toxicity and biodegradation of phenolics: recent progress and future outlook. *Environ Technol Innov* 27:102423. <https://doi.org/10.1016/j.eti.2022.102423>
- Parvin F, Sultana N, Habib SMA, Bhoumik NC (2017) Gamma irradiation and steam pretreatment of jute stick powder for the enhancement of dye adsorption efficiency. *Appl Water Sci* 7(7):3503–3510. <https://doi.org/10.1007/s13201-017-0617-2>
- Patel S, Han J, Qiu W, Gao W (2015) Synthesis and characterisation of mesoporous bone char obtained by pyrolysis of animal bones, for environmental application. *J Environ Chem Eng* 3(4):2368–2377. <https://doi.org/10.1016/j.jece.2015.07.031>
- Pérez Jiménez VA, Hernández-Montoya V, Ramírez-Montoya LA, Castillo-Borja F, Tovar-Gómez R, Montes-Morán MA (2021) Adsorption of impurities from nickel-plating baths using commercial sorbents to reduce wastewater discharges. *J Environ Manag* 284:112024. <https://doi.org/10.1016/j.jenvman.2021.112024>
- Piccirillo C (2023) Preparation, characterisation and applications of bone char, a food waste-derived sustainable material: a review. *J Environ Manag* 339:117896. <https://doi.org/10.1016/j.jenvman.2023.117896>
- Piccirillo C, Moreira IS, Novais RM, Fernandes AJS, Pullar RC, Castro PML (2017) Biphasic apatite-carbon materials derived from pyrolysed fish bones for effective adsorption of persistent pollutants and heavy metals. *J Environ Chem Eng* 5(5):4884–4894. <https://doi.org/10.1016/j.jece.2017.09.010>
- Pombo F, Magrini A, Szklo A (2011) Technology roadmap for wastewater reuse in petroleum refineries in Brazil. Environmental management in practice. InTech
- Radovic LR, Moreno-Castilla C, Rivera-Utrilla J (2000) Carbon materials as adsorbents in aqueous solutions. Chemistry & physics of carbon. CRC Press, pp 247–426
- Randall DG, Nathoo J, Lewis AE (2011) A case study for treating a reverse osmosis brine using Eutectic Freeze Crystallization—Approaching a zero waste process. *Desalination* 266(1–3):256–262. <https://doi.org/10.1016/j.desal.2010.08.034>
- Rashid R, Shafiq I, Akhter P, Iqbal MJ, Hussain M (2021) A state-of-the-art review on wastewater treatment techniques: the effectiveness of adsorption method. *Environ Sci Pollut Res* 28(8):9050–9066. <https://doi.org/10.1007/s11356-021-12395-x>
- Reynolds TD, Richards PAC (1995) Unit operations and processes in environmental engineering, 2nd edn. PWS Publishing Company, Boston

- Rezaee A, Rangkooy H, Jonidi-Jafari A, Khavanin A (2013) Surface modification of bone char for removal of formaldehyde from air. *Appl Surf Sci* 286:235–239. <https://doi.org/10.1016/j.apsusc.2013.09.053>
- Ribeiro MV (2011) Uso de carvão de osso bovino na defluoretação de água para uso em abastecimento público. Federal University of Minas Gerais
- Robinson T, Chandran B, Nigam P (2002) Effect of pretreatments of three waste residues, wheat straw, corncobs and barley husks on dye adsorption. *Bioresour Technol* 85(2):119–124. [https://doi.org/10.1016/S0960-8524\(02\)00099-8](https://doi.org/10.1016/S0960-8524(02)00099-8)
- Rocha SD, Ribeiro MV, Viana PD, Mansur MB (2012) Bone char: an alternative for the removal of diverse organic and inorganic compounds from industrial wastewaters. Application of adsorbents for water pollution control. Bentham Science Publishers, pp 502–522
- Rojas-Mayorga CK, Bonilla-Petriciolet A, Aguayo-Villarreal IA, Hernández-Montoya V, Moreno-Virgen MR, Tovar-Gómez R, Montes-Morán MA (2013) Optimization of pyrolysis conditions and adsorption properties of bone char for fluoride removal from water. *J Anal Appl Pyrolysis* 104:10–18. <https://doi.org/10.1016/j.jaap.2013.09.018>
- Rojas-Mayorga CK, Bonilla-Petriciolet A, Sánchez-Ruiz FJ, Moreno-Pérez J, Reynel-Ávila HE, Aguayo-Villarreal IA, Mendoza-Castillo DI (2015) Breakthrough curve modeling of liquid-phase adsorption of fluoride ions on aluminum-doped bone char using micro-columns: Effectiveness of data fitting approaches. *J Mol Liq* 208:114–121. <https://doi.org/10.1016/j.molliq.2015.04.045>
- Santos NT, Landers R, da Silva MG, Vieira MG (2020) Adsorption of gold ions onto sericin and alginate particles chemically crosslinked by proanthocyanidins: a complete fixed-bed column study. *Ind Eng Chem Res* 59(1):318–328. <https://doi.org/10.1021/acs.iecr.9b04914>
- Sellaoui L, Dhaouadi F, Reynel-Ávila HE, Mendoza-Castillo DI, Bonilla-Petriciolet A, Trejo-Valencia R, Taamalli S, Louis F, El Bakali A, Chen Z (2021) Physicochemical assessment of anionic dye adsorption on bone char using a multilayer statistical physics model. *Environ Sci Pollut Res* 28(47):67248–67255. <https://doi.org/10.1007/s11356-021-15264-9>
- Silva LGM, Moreira FC, Souza AAU, Souza SM, Boaventura RAR, Vilar VJP (2018) Chemical and electrochemical advanced oxidation processes as a polishing step for textile wastewater treatment: a study regarding the discharge into the environment and the reuse in the textile industry. *J Clean Prod* 198:430–442. <https://doi.org/10.1016/j.jclepro.2018.07.001>
- Souza AGM, De Souza FB, de Ulson Souza AA (2012) Application of individual and simultaneous ozonation and adsorption processes in batch and fixed-bed reactors for phenol removal. *Ozone Sci Eng* 34(4):259–268. <https://doi.org/10.1080/01919512.2012.688711>
- Tang F, Hu H-Y, Sun L-J, Sun Y-X, Shi N, Crittenden JC (2016) Fouling characteristics of reverse osmosis membranes at different positions of a full-scale plant for municipal wastewater reclamation. *Water Res* 90:329–336. <https://doi.org/10.1016/j.watres.2015.12.028>
- Thomas HC (1944) Heterogeneous Ion exchange in a flowing system. *J Am Chem Soc* 66(10):1664–1666. <https://doi.org/10.1021/ja01238a017>
- Thommes M, Kaneko K, Neimark AV, Olivier JP, Rodriguez-Reinoso F, Rouquerol J, Sing KSW (2015) Physisorption of gases, with special reference to the evaluation of surface area and pore size distribution (IUPAC Technical Report). *Pure Appl Chem* 87(9–10):1051–1069. <https://doi.org/10.1515/pac-2014-1117>
- Tovar-Gómez R, Moreno-Virgen MR, Dena-Aguilar JA, Hernández-Montoya V, Bonilla-Petriciolet A, Montes-Morán MA (2013) Modeling of fixed-bed adsorption of fluoride on bone char using a hybrid neural network approach. *Chem Eng J* 228:1098–1109. <https://doi.org/10.1016/j.cej.2013.05.080>
- Turek M, Mitko K, Piotrowski K, Dydo P, Laskowska E, Jakóbk-Kolon A (2017) Prospects for high water recovery membrane desalination. *Desalination* 401:180–189. <https://doi.org/10.1016/j.desal.2016.07.047>
- United Nations (2015) Transforming our world: the 2030 Agenda for Sustainable Development. In: Gen. Assem. <https://sustainabledevelopment.un.org/content/documents/21252030Agenda> for Sustainable Development web.pdf. Accessed 25 Jul 2020
- Valverde SA, Azevedo JCV, França AB, Santos IJB, Naves FL, Mesquita PL (2022) Removal of boron from water by batch adsorption onto bovine bone char: optimization, kinetics and equilibrium. *Int J Environ Sci Technol*. <https://doi.org/10.1007/s13762-022-04643-5>
- Villela-Martínez DE, Leyva-Ramos R, Aragón-Piña A, Navarro-Tovar R (2020) Arsenic elimination from water solutions by adsorption on bone char. Effect of operating conditions and removal from actual drinking water. *Water Air Soil Pollut* 231(5):201. <https://doi.org/10.1007/s11270-020-04596-w>
- Vourch M, Balanec B, Chaufer B, Dorange G (2008) Treatment of dairy industry wastewater by reverse osmosis for water reuse. *Desalination* 219(1–3):190–202. <https://doi.org/10.1016/j.desal.2007.05.013>
- Wang S, Wu X, Xu S, Leng Q, Jin D, Wang P, Dong F, Wu D (2023) Energetic evaluation of phenol wastewater treatment by reverse electro dialysis reactor using different anodes. *J Environ Manag* 329:117089. <https://doi.org/10.1016/j.jenvman.2022.117089>
- Worch E (2012) Adsorption technology in water treatment: fundamentals, processes, and modeling. Walter de Gruyter, Dresden
- Xavier ALP (2018) Modelagem e otimização da adsorção de metais tóxicos em coluna de leito-fixado utilizando bagaço de cana-de-açúcar modificado quimicamente como adsorvente. Universidade Federal de Ouro Preto
- Xu C, Shi S, Wang X, Zhou H, Wang L, Zhu L, Zhang G, Xu D (2020) Electrospun SiO₂-MgO hybrid fibers for heavy metal removal: characterization and adsorption study of Pb(II) and Cu(II). *J Hazard Mater* 381:120974. <https://doi.org/10.1016/j.jhazmat.2019.120974>
- Xu Z, Cai J, Pan B (2013) Mathematically modeling fixed-bed adsorption in aqueous systems. *J Zhejiang Univ Sci A* 14(3):155–176. <https://doi.org/10.1631/jzus.A1300029>
- Yan G, Viraraghavan T, Chen M (2001) A new model for heavy metal removal in a biosorption column. *Adsorpt Sci Technol* 19(1):25–43. <https://doi.org/10.1260/0263617011493953>
- Yang Y, Cannon FS (2022) Biomass activated carbon derived from pine sawdust with steam bursting pretreatment; perfluorooctanoic acid and methylene blue adsorption. *Bioresour Technol* 344:126161. <https://doi.org/10.1016/j.biortech.2021.126161>
- Yang Z, Dong Y, Meng X, Yang X, Hu R, Liu Y, Wu J (2022) Nitrogen-functionalized bone chars with developed surface area for efficient adsorption of multiple aquatic pollutants. *Colloids Surf A Physicochem Eng Asp* 647:129061. <https://doi.org/10.1016/j.colsurfa.2022.129061>
- Yoon YH, Nelson JH (1984) Application of gas adsorption kinetics I. A theoretical model for respirator cartridge service life. *Am Ind Hyg Assoc J* 45(8):509–516. <https://doi.org/10.1080/15298668491400197>

Publisher's Note Springer Nature remains neutral with regard to jurisdictional claims in published maps and institutional affiliations.

Springer Nature or its licensor (e.g. a society or other partner) holds exclusive rights to this article under a publishing agreement with the author(s) or other rightsholder(s); author self-archiving of the accepted manuscript version of this article is solely governed by the terms of such publishing agreement and applicable law.